

# Modeling Two-Scale Degradation with Heterogeneity: A Unified Random-Effects Inverse Gaussian Framework

Liangliang Zhuang<sup>a</sup>, Yizhong Ma<sup>a</sup>, Guanqi Fang<sup>b,c</sup>, Ancha Xu<sup>b,c,d,\*</sup>

<sup>a</sup>*School of Economics and Management, Department of Management Science and Engineering, Nanjing University of Science and Technology, Nanjing, 210094, China*

<sup>b</sup>*School of Statistics and Data Science, Zhejiang Gongshang University, Hangzhou 310018, China*

<sup>c</sup>*Collaborative Innovation Center of Statistical Data Engineering, Technology & Application Zhejiang Gongshang University, Hangzhou, China*

<sup>d</sup>*Laboratory for Statistical Monitoring and Intelligent Governance of Common Prosperity*

---

## Abstract

Accurate modeling of product degradation is essential for reliable life prediction and maintenance planning. In many applications, degradation is jointly driven by age (calendar time) and usage (cumulative operation), and further complicated by unit-to-unit heterogeneity due to manufacturing or environmental variations. While existing models often focus on single-scale processes or assume homogeneous systems, few frameworks can flexibly accommodate both two scales and population-level variability. This paper proposes a unified two-scale degradation model based on additive reparameterized inverse Gaussian processes with random effects. The model captures monotonic degradation under the joint influence of age and usage, and introduces two forms of random effects to flexibly capture varying degrees of heterogeneity across units. It provides closed-form expressions for failure time distributions, enabling efficient reliability analysis. Two inference methods are developed: (i) a maximum likelihood estimator via an expectation-maximization algorithm with bootstrap intervals, and (ii) a Bayesian approach using Hamiltonian Monte Carlo sampling. Simulation studies confirm the accuracy and robustness of the proposed estimators and highlight the risks of model misspecification in reliability assessment. A real-world case study on outdoor coating degradation further demonstrates the model's practical applicability. An open-source R package is provided to support implementation, with additional materials available online.

*Keywords:* Inverse Gaussian process; Two scales; Degradation; Random effects

---

---

\*Corresponding author: xuancha@mail.zjgsu.edu.cn

# 1. Introduction

## 1.1. Background

With the increasing complexity of modern operating environments, the factors driving product performance degradation have become increasingly diverse. Over a product’s life-cycle, degradation may result from both calendar time (age-based aging) and cumulative operational usage (usage-based aging). Without timely intervention, such degradation can lead to reduced efficiency, suboptimal performance, or even catastrophic failure. Therefore, accurate degradation modeling and predictive maintenance strategies are critical to ensuring system reliability and safety (Wang and Tang, 2025; Zhao et al., 2025).

In practice, both *age-based* and *usage-based* degradation mechanisms often coexist and interact (Wang et al., 2020; Peng et al., 2024). Age-based degradation refers to natural deterioration over time due to material fatigue, corrosion, or environmental exposure. Usage-based degradation, by contrast, results from cumulative loads, repeated stress, or operational cycles. For instance, electric vehicle batteries experience age-based capacity fade as well as usage-driven increases in internal resistance. Capturing such dual degradation pathways requires models that account for both temporal and operational scales simultaneously.

Moreover, real-world systems often exhibit unit-to-unit variability caused by manufacturing imperfections, operating conditions, or environmental heterogeneity (Xu and Wang, 2025). Ignoring such differences may lead to biased reliability estimates and misleading maintenance decisions. As a result, degradation models must not only incorporate multiple time scales but also account for cross-unit heterogeneity in degradation behavior. The following example further illustrates this research context.

## 1.2. Motivation

This example comes from a five-year outdoor experiment conducted by the national institute of standards and technology (Gu et al., 2009). In this study, researchers placed coating material samples in outdoor chambers to observe their degradation under environmental factors such as ultraviolet (UV) radiation exposure. By monitoring the attenuation of the  $1250\text{ cm}^{-1}$  peak in Fourier transform infrared spectroscopy, they assessed the material’s degradation (Hong et al., 2015). In this process, degradation accumulated gradually over time (time-based aging), while UV radiation accelerated polymer chain breakdown, molecular weight reduction, and mechanical weakening. Thus, cumulative UV exposure serves as a key indicator of usage-based aging.

Figure 1 shows the degradation paths of two sample groups across calendar time and cumulative UV exposure (both scaled by  $\times 10^2$  for UV exposure and degradation values), along with projections of each pair of axes. The figure reveals that degradation increases monotonically with calendar time, while cumulative UV exposure grows nonlinearly. Although the degradation paths within each group (e.g., G9) show limited variation, small inter-unit differences remain, reflecting potential heterogeneity in practical settings.

These observations raise key questions: Can a model be developed to jointly capture degradation driven by both age and usage? Can it account for the combined and scale-dependent effects of calendar time and cumulative UV exposure while remaining flexible enough to incorporate unit-to-unit variability? To address these challenges, this article proposes a two-scale monotonic degradation model with random effects, along with methods for parameter estimation and reliability analysis.

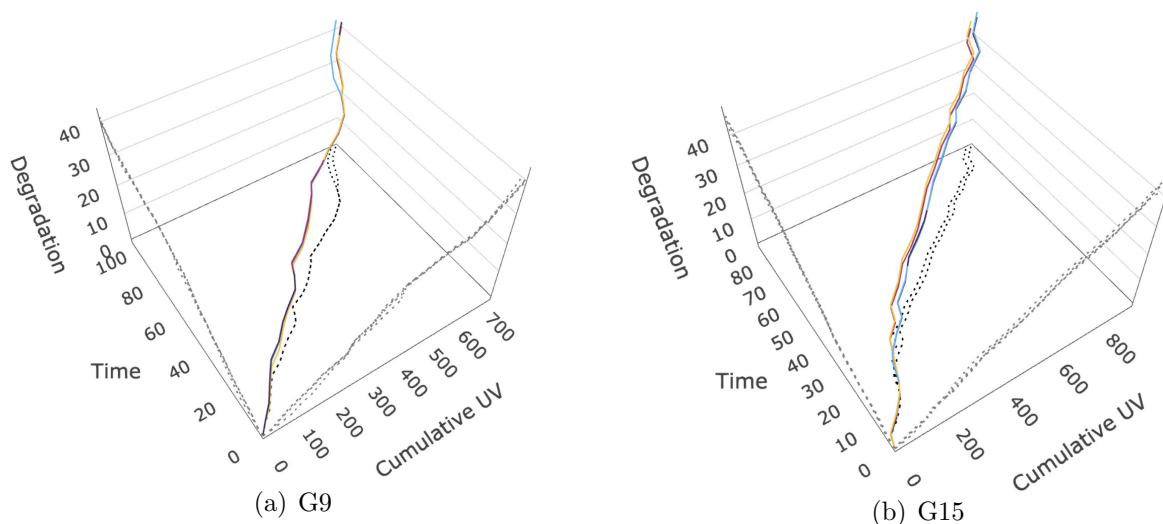


Figure 1: Degradation of the coating material over calendar time and cumulative UV exposure.

### 1.3. Related literature

Traditional degradation modeling primarily relies on general path models (Si et al., 2013; Lu et al., 2020). While effective in certain contexts, these models treat degradation as a deterministic process, ignoring inherent randomness. This simplification limits their ability to capture the true degradation paths of products, reducing their suitability for complex degradation behaviors (Zhai et al., 2023). To overcome these limitations, stochastic process

models, classified as either non-monotonic or monotonic based on degradation increment properties, have been widely adopted in degradation modeling.

- i) **Non-monotonic degradation processes:** Common models include the Wiener process (Wang et al., 2023a; Fang and Pan, 2024), fractional Lévy motion (Zhang et al., 2021; Asgari et al., 2024), and the Student-t process (Peng and Cheng, 2020; Xu et al., 2025), which are suitable for degradation processes with fluctuations or non-monotonic behavior (Zhang et al., 2018). These models have been extensively studied and applied in engineering applications. For instance: Hu et al. (2020) developed a Wiener process model with random effects for online RUL prediction, using data from lead-acid batteries and digital communication systems. Wang et al. (2023b) applied an autoregressive model with a Wiener process to simulate stochastic degradation rates in rechargeable battery and bearing data. Liu et al. (2022) introduced a fractional Lévy motion-based method for RUL prediction, capturing long-range dependence in lithium-ion battery degradation. Li et al. (2023) further extended this with adaptive diffusion coefficients and nonlinear drift, applying it to truck rear axle data. Peng and Cheng (2020) proposed a robust Student-t process model for lifetime assessment of highly reliable products, illustrated by resistance, train wheel, and light-emitting diode (LED) degradation data.
- ii) **Monotonic degradation processes:** Common models include the gamma process (Zhou et al., 2023; Song and Cui, 2022) and the inverse Gaussian (IG) process (Wang and Xu, 2010; Ye and Chen, 2014; Zhuang et al., 2024), which are effective in characterizing cumulative degradation. These models are also widely applied in practical scenarios. For instance: Wang et al. (2021) proposed a random-effects gamma degradation model and applied it to laser data and Device-B data. Both Ling et al. (2019) and Lin et al. (2021) developed gamma process models for two-phase degradation—Ling et al. (2019) applied the model to LED data, while Lin et al. (2021) used it to cycle aging data from lithium batteries. Peng et al. (2014) introduced a Bayesian framework using the IG process for degradation analysis, validating it with monotonic datasets. Extending this model, Fang et al. (2022) developed a multivariate IG model that accounts for performance dependencies and product heterogeneity, applied to coating and fatigue crack-size data.

However, the aforementioned studies primarily address degradation indexed by a single

scale. To avoid confusion, multivariate degradation models are not equivalent to multi-scale degradation models: although multivariate models are statistically multidimensional, they still operate on a single physical scale—typically time—because all degradation signals evolve along a common temporal axis. Few considering a two-scale approach. For instance, [Zhang et al. \(2017\)](#) introduced a linear Wiener process model to capture degradation across both age and usage scales, which [Pei et al. \(2019\)](#) later extended to a nonlinear form for gyroscope data. Nevertheless, these studies assume a constant usage rate and overlook dependencies between the two scales. To address these issues, [Zhai et al. \(2023\)](#) proposed an innovative two-scale model that combines two independent Wiener processes,  $\mathcal{X}(t)$  and  $\mathcal{Z}(u)$ , representing degradation caused by the age scale  $t$  and the usage scale  $u$ , respectively. The degradation from these two scales combines into the observed degradation path,  $\mathcal{Y}(t, u) = \mathcal{X}(t) + \mathcal{Z}(u)$ , which follows a normal distribution given fixed  $t$  and  $u$  due to the property of Wiener process. This model provides two key advantages: (i) a clear physical interpretation of how both scales jointly affect product lifetime, and (ii) tractable properties, including a closed-form lifetime distribution, facilitating application in reliability prediction. Despite advancements, monotonic process-based two-scale models may be particularly suited for analyzing systems with monotonic degradation, such as wear in power shift steering transmissions ([Song and Cui, 2022](#)), operational currents of GaAs lasers ([Zhou et al., 2023](#)), and the example in Section 1.2. Monotonic models are generally more effective at capturing cumulative degradation patterns and enhancing reliability estimates, yet research in this area remains limited. Moreover, under the two-scale setting, unit-to-unit heterogeneity has not been sufficiently addressed. While recent studies have incorporated random effects to capture such heterogeneity in both monotonic and nonmonotonic degradation processes ([Zhai et al., 2025](#); [Fan et al., 2023](#); [Zhou et al., 2023](#)), most of these works remain within single-scale frameworks and rarely consider cross-scale dependence. Neglecting heterogeneity—arising from variations in material properties, manufacturing processes, or environmental exposure—may lead to biased inference and reduced prediction accuracy. This motivates the development of a unified two-scale model with shared random effects, which jointly characterizes age–usage dependence and unit-level variability within a coherent probabilistic framework.

Table 1: Comparison of representative degradation modeling frameworks.

Model	Scale dependency	Random effects	Path monotonicity	References
Single-scale	-	No	Monotonic	• <a href="#">Lin et al. (2021)</a>
		Yes	Monotonic	• <a href="#">Fang et al. (2022)</a>
		Yes	Non-monotonic	• <a href="#">Zhai et al. (2025)</a>
Two-scale	Independent	No	Non-monotonic	• <a href="#">Zhang et al. (2017)</a>
	Dependent	No	Non-monotonic	• <a href="#">Zhai et al. (2023)</a>
	Dependent	Yes	Monotonic	• This paper

#### 1.4. Contribution and overview

Table 1 summarizes representative degradation modeling frameworks in terms of scale dependency, random effects, and degradation-path monotonicity. As shown, single-scale models are indexed by a single scale (typically calendar time) and partially account for unit-level heterogeneity. Two-scale models have been developed to incorporate both calendar time and usage, but most existing studies either assume independence between the two scales, consider nonmonotonic degradation paths, or fail to capture unit-to-unit variability. In contrast, this study proposes a dependent two-scale framework that integrates shared random effects to represent cross-scale interactions and individual heterogeneity, while preserving the monotonic characteristics of physical degradation. The main contributions of this study can be summarized as follows:

- A unified dependent two-scale degradation framework is developed based on the reparameterized inverse Gaussian (rIG) process, capturing monotonic degradation jointly driven by time and usage while accounting for unit-level heterogeneity. Existing single-scale and independent two-scale models are encompassed as special cases.
- Statistical properties are derived, yielding a closed-form lifetime distribution that ensures computational efficiency for reliability assessment.
- Two complementary estimation approaches are proposed: maximum likelihood estimation via an expectation–maximization (EM) algorithm and Bayesian inference.

- An open-source R package, `r2IGP`, is developed to facilitate its implementation and reliability analysis in practice.

The remainder of this article is organized as follows. Section 2 discusses the model formulation and reliability analysis. Section 3.1 introduces the data and likelihood function, while Sections 3.2 and 3.3 detail the EM algorithm and the bootstrap method, respectively. Section 4 evaluates inference accuracy and the impact of model misspecification through simulations. Section 5 applies the proposed methodology to coating material data, and Section 6 concludes the study.

## 2. Model formulation

This section begins by defining the rIG process and applying it to the two-scale degradation model with random effects, along with other extended models (see Section 2.1). It then presents the theoretical properties and failure time distribution of the proposed model (see Section 2.2), followed by a reliability analysis (see Section 2.3).

### 2.1. Two-scale rIG processes

Consider a stochastic process  $\mathcal{J}(u)$ , defined as an rIG process  $rIG(\Lambda(u), \gamma)$ , if it satisfies the following properties: (i)  $\mathcal{J}(0) = 0$  with probability 1; (ii)  $\mathcal{J}(u)$  has independent increments, that is, for any  $u_4 > u_3 \geq u_2 > u_1 \geq 0$ , the increments  $\mathcal{J}(u_4) - \mathcal{J}(u_3)$  and  $\mathcal{J}(u_2) - \mathcal{J}(u_1)$  are independent; (iii) For all  $u > v \geq 0$ , the increment  $\mathcal{J}(u) - \mathcal{J}(v)$  follows an rIG distribution  $rIG(\Lambda(u) - \Lambda(v), \gamma)$ . In this context,  $\Lambda(\cdot)$  is a non-decreasing function satisfying  $\Lambda(0) = 0$ , representing the drift parameter, and  $\gamma$  is the dispersion parameter. The probability density function (PDF) of  $rIG(\theta, \gamma)$  is defined as

$$f_{rIG}(y; \theta, \gamma) = \frac{\theta}{\sqrt{2\pi}} y^{-3/2} \exp \left\{ -\frac{1}{2} \left( \frac{\theta}{\sqrt{y}} - \gamma \sqrt{y} \right)^2 \right\}, \quad y > 0, \theta > 0, \gamma > 0. \quad (1)$$

Note that the rIG distribution,  $rIG(\theta, \gamma)$ , relates to the traditional IG distribution,  $IG(a, b)$ , through the parameter transformations  $a = \theta/\gamma$  and  $b = \theta^2$ . Specifically, if  $\mathcal{Y}_1 \sim rIG(\theta_1, \gamma)$  and  $\mathcal{Y}_2 \sim rIG(\theta_2, \gamma)$  are two independent random variables, then their summation,  $\mathcal{Y} = \mathcal{Y}_1 + \mathcal{Y}_2$ , also follows an rIG distribution  $rIG(\theta_1 + \theta_2, \gamma)$  (Zhuang et al., 2024).

Motivated by this additive closure, we construct an additive two-scale rIG model for monotonic degradation. For a unit  $i, i = 1, 2, \dots, n$ , the degradation process  $\mathcal{Y}_i(t, u)$  is represented by two scales  $t > 0$  and  $u > 0$ , and is formulated as

$$\mathcal{Y}_i(t, u) = \mathcal{X}_i(t) + \mathcal{Z}_i(u), \quad (2)$$

with  $\mathcal{X}_i(t) \sim r\mathcal{IG}(\Lambda^t(t), \gamma)$ , and  $\mathcal{Z}_i(u) \sim r\mathcal{IG}(\Lambda^u(u), \gamma)$ . Here,  $\mathcal{X}_i(t)$  and  $\mathcal{Z}_i(u)$  are independent rIG processes that both follow the form described in (1) and share the same dispersion parameter  $\gamma$ , assumed to reflect the underlying failure mechanism of the product. The functions  $\Lambda^t(t)$  and  $\Lambda^u(u)$  act as the drift parameters for  $\mathcal{X}_i(t)$  and  $\mathcal{Z}_i(u)$ , respectively. In practical applications, the specific functional form of  $\Lambda(\cdot)$  can be identified based on engineering knowledge or empirical analysis.

Note that the proposed two-scale model adopts an additive structure, which represents the cumulative contributions of calendar time and usage to degradation. In many physicochemical aging mechanisms (e.g., corrosion progression, coating photodegradation, and fatigue damage accumulation), different degradation drivers accumulate through distinct damage pathways (Wang, 2023). This makes the additive formulation a reasonable approximation for a broad class of degradation processes. In addition, the additive form leads to closed-form reliability expressions and improves parameter identifiability by avoiding the confounding that often arises in multiplicative or interaction-based models. Nevertheless, when strong interactions exist between the two scales, the additive form may become inadequate, and multiplicative or interaction models can serve as potential extensions. A brief discussion of such possible extensions is provided in the Section 6.

Due to the diversity in manufacturing processes, material properties, and operating environments, products often exhibit unique degradation characteristics. To capture this heterogeneity among products, we model  $\gamma$  as a random variable with a normal distribution, expressed as  $\gamma_i \sim \mathcal{N}(\kappa, \sigma^2)$ . The probability of  $\gamma_i$  being negative becomes negligibly small when  $\kappa/\sigma^2 \gg 0$ , which is typically a reasonable assumption in practice (Peng and Cheng, 2020). In summary, the proposed model labeled as  $M_0$  is formulated as follows:

$$M_0 : \begin{cases} \mathcal{Y}_i(t, u) = \mathcal{X}_i(t) + \mathcal{Z}_i(u), \\ \mathcal{X}_i(t) \mid \gamma_i \sim r\mathcal{IG}(\Lambda^t(t), \gamma_i), \\ \mathcal{Z}_i(u) \mid \gamma_i \sim r\mathcal{IG}(\Lambda^u(u), \gamma_i), \\ \gamma_i \sim \mathcal{N}(\kappa, \sigma^2). \end{cases} \quad [M_0]$$

Model  $[M_0]$  draws inspiration from the degradation mechanisms observed in physical systems, such as coating materials and batteries. Here,  $\mathcal{X}_i(t)$  represents age-based degradation, capturing processes like material fatigue that progress over calendar time  $t$ , while  $\mathcal{Z}_i(u)$  captures usage-based degradation, reflecting wear due to cumulative operational cycles. This two-scale framework enables independent modeling of each degradation path while capturing their combined influence on product reliability. The structure effectively addresses the complexity of real-world product degradation mechanisms, making it particularly suitable for predicting failures with both age- and usage-based deterioration.

To accommodate the practical needs of degradation modeling in various engineering scenarios, the proposed model  $[M_0]$  is formulated as a unified two-scale stochastic degradation framework. It not only provides full parameter flexibility but also encompasses four meaningful model variants derived from real-world considerations. These variants are constructed by adjusting two key dimensions: (i) the degradation scale involved (single or dual), and (ii) the presence or absence of unit-to-unit heterogeneity (i.e., random effects). Such structural differences correspond to typical degradation settings observed in practice, including systems affected by multiple degradation mechanisms or those exhibiting variability due to manufacturing inconsistencies. Table 2 summarizes the proposed unified framework and its representative variants, including both newly introduced models and existing formulations from the literature. To our knowledge, this is the first work to systematically organize these models under a unified rIG-based framework.

Specifically, model  $M_1$  assumes no random effects across units, implying a common dispersion parameter ( $\gamma_1 = \dots = \gamma_n$ ). In this case, the variability in degradation can be sufficiently explained by the scale-specific processes  $\mathcal{X}_i(t)$  and  $\mathcal{Z}_i(u)$  alone. This model is suited for highly standardized systems with minimal unit-level differences, such as precision electronic components or transistor arrays tested under controlled laboratory conditions, where environmental and manufacturing variability can be considered negligible. Notably, the two-scale Wiener process model proposed in [Zhai et al. \(2023\)](#) adopts a similar additive structure to describe degradation across age and usage scales. Their formulation models  $\mathcal{X}(t)$  and  $\mathcal{Z}(u)$  as independent Wiener processes with fixed parameters shared across all units. In contrast, our model builds upon this idea by extending it to a broader class of inverse Gaussian processes and further incorporating random effects to capture unit-level heterogeneity.

Model  $M_2$  adopts the identity-trick approach to capture mild heterogeneity among

units, where variations fluctuate around a shared baseline. The scaling parameter  $\kappa$  controls the overall variability, while the random effect  $\gamma_i \sim \mathcal{N}(1, \sigma^2)$  models deviations from the common center. This formulation is appropriate for systems with moderate batch-level variability, such as LED modules or lithium-ion battery packs across different production runs. Although similar strategies have been widely applied in single-scale gamma processes (Song and Cui, 2022; Barui et al., 2024; Zhou et al., 2023), this study is the first to extend them to the rIG-based setting.

We also introduce two single-scale degradation models, with or without random effects, denoted as  $M_3$  and  $M_4$ . In these cases, the scale function  $\Lambda(t)$  refers to either calendar time or accumulated usage. Such IG-based models are frequently used in practice (Ye and Chen, 2014; Peng, 2015), and are well-suited for systems where degradation is predominantly driven by a single mechanism. For instance, the capacity fade of lithium-ion batteries during storage is primarily governed by calendar aging, while wear degradation in components such as bearings or cutting tools is mainly usage-driven. In these scenarios, single-scale models offer a simpler structure that facilitates estimation and maintenance decision-making.

Overall, models  $M_1$ – $M_4$  are not merely structural reductions of the general model  $[M_0]$ , but are purposefully designed to reflect representative degradation behaviors encountered in engineering applications. By systematically presenting these model variants under a unified framework, we enhance modeling flexibility and provide practitioners with clear guidance for model selection and interpretation.

## 2.2. Theoretical properties

Based on the definition, the mean and variance of the rIG distribution are  $\theta/\gamma$  and  $\theta/\gamma^3$ , respectively. Utilizing the summation property of the rIG distribution, the properties of  $\mathcal{Y}_i(t, u)$  in model  $[M_0]$ , given  $\gamma_i$ , are summarized in Lemma 1.

**Lemma 1.** *Conditioned on  $\gamma_i$ ,  $\mathcal{Y}_i(t, u) \mid \gamma_i \sim r\mathcal{IG}(\Lambda^t(t) + \Lambda^u(u), \gamma_i)$ . The expectation and variance are given by*

$$\mathbb{E}[\mathcal{Y}_i(t, u) \mid \gamma_i] = \frac{\Lambda^t(t) + \Lambda^u(u)}{\gamma_i} \quad \text{and} \quad \text{Var}(\mathcal{Y}_i(t, u) \mid \gamma_i) = \frac{\Lambda^t(t) + \Lambda^u(u)}{\gamma_i^3}.$$

To derive the unconditional distribution of  $\mathcal{Y}_i(t, u)$ ,  $\gamma_i$  is integrated out. The result is presented in Proposition 1, with the proof provided in [supplementary Section S1.1](#).

Table 2: Representative models under the unified two-scale framework.

Model	Scales	Random-effects	Formulation	Reference
$M_0$	$Y_i(t, u)$	$\gamma_i \sim \mathcal{N}(\kappa, \sigma^2)$	$X_i(t) \mid \gamma_i \sim r\mathcal{IG}(\Lambda^t(t), \gamma_i)$ $Z_i(u) \mid \gamma_i \sim r\mathcal{IG}(\Lambda^u(u), \gamma_i)$	–
$M_1$	$Y_i(t, u)$	–	$X_i(t) \sim r\mathcal{IG}(\Lambda^t(t), \gamma)$ $Z_i(u) \sim r\mathcal{IG}(\Lambda^u(u), \gamma)$	• Zhai et al. (2023)
$M_2$	$Y_i(t, u)$	$\gamma_i \sim \mathcal{N}(1, \sigma^2)$	$X_i(t) \mid \gamma_i \sim r\mathcal{IG}(\Lambda^t(t), \kappa\gamma_i)$ $Z_i(u) \mid \gamma_i \sim r\mathcal{IG}(\Lambda^u(u), \kappa\gamma_i)$	–
$M_3$	$Y_i(t)$	$\gamma_i \sim \mathcal{N}(\kappa, \sigma^2)$	$Y_i(t) \sim r\mathcal{IG}(\Lambda(t), \gamma_i)$	• Song and Cui (2022) • Barui et al. (2024) • Zhou et al. (2023)
$M_4$	$Y_i(t)$	–	$Y_i(t) \sim r\mathcal{IG}(\Lambda(t), \gamma)$	• Ye and Chen (2014) • Peng (2015)

\* All models are formulated under the unified two-scale framework. Models  $M_0$  and  $M_2$  are newly proposed in this study, while  $M_1$ ,  $M_3$ , and  $M_4$  correspond to related forms previously discussed in the literature.

**Proposition 1.** *The unconditional distribution of  $\mathcal{Y}_i(t, u)$  is given by*

$$f_{\mathcal{Y}_i(t, u)}(y) = y^{-3/2} \frac{\Lambda_i(t, u)}{\sqrt{2\pi(1 + y\sigma^2)}} \exp \left[ -\frac{\kappa^2 y - 2\kappa\Lambda_i(t, u) + \Lambda_i(t, u)^2/y}{2(y\sigma^2 + 1)} \right], \quad (3)$$

where  $\Lambda_i(t, u) = \Lambda_i^t(t) + \Lambda_i^u(u)$ . Based on Lemma 1 and by applying the laws of total expectation and total variance, the unconditional mean and variance of  $\mathcal{Y}_i(t, u)$  are given as follows:

$$\begin{aligned} \mathbb{E}[\mathcal{Y}_i(t, u)] &= \Lambda(t, u) \mathbb{E}(\gamma_i^{-1}), \\ \text{Var}[\mathcal{Y}_i(t, u)] &= \Lambda(t, u) \mathbb{E}(\gamma_i^{-3}) + \Lambda(t, u)^2 \left\{ \mathbb{E}(\gamma_i^{-2}) - [\mathbb{E}(\gamma_i^{-1})]^2 \right\}. \end{aligned} \quad (4)$$

The shared random effect  $\gamma_i$  induces a nonzero cross-scale covariance and hence statistical dependence between the two components.

$$\begin{aligned} \text{Cov}(\mathcal{X}_i(t), \mathcal{Z}_i(u)) &= \Lambda^t(t)\Lambda^u(u) \text{Var}(\gamma_i^{-1}), \\ \text{Corr}(\mathcal{X}_i(t), \mathcal{Z}_i(u)) &= \frac{\sqrt{\Lambda^t(t)\Lambda^u(u)} \text{Var}(\gamma_i^{-1})}{\sqrt{[\mathbb{E}(\gamma_i^{-3}) + \Lambda^t(t) \text{Var}(\gamma_i^{-1})][\mathbb{E}(\gamma_i^{-3}) + \Lambda^u(u) \text{Var}(\gamma_i^{-1})]}}. \end{aligned} \quad (5)$$

According to Proposition 1, the introduction of the random effect  $\gamma_i$  explicitly captures unit-level heterogeneity and mediates the interaction between the two degradation scales.

However, since the inverse moments  $\mathbb{E}(\gamma_i^{-r})$  ( $r = 1, 2, 3$ ) diverge at  $\gamma_i = 0$ , these expectations are not mathematically defined when  $\gamma_i \sim \mathcal{N}(\kappa, \sigma^2)$ . To address this, we approximate these expectations using Monte Carlo (MC) simulation. Specifically, when  $\kappa/\sigma$  is large, most  $\gamma_i$  samples are positive, making this approach viable. A large number of positive  $\gamma_i$  samples are generated from  $\mathcal{N}(\kappa, \sigma^2)$ , and their reciprocal sample means are used as approximations.

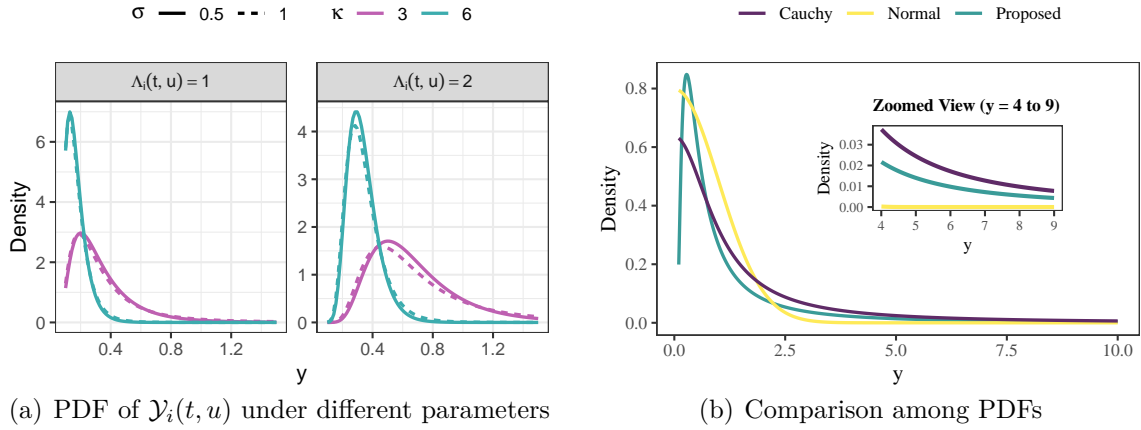


Figure 2: Properties of the unconditional PDF of  $\mathcal{Y}_i(t, u)$ , and comparison with other baseline distributions.

Figure 2 illustrates the properties of the unconditional PDF of  $\mathcal{Y}_i(t, u)$  under various parameter settings. In Figure 2(a), the standard deviation parameter  $\sigma$  is represented by line type, the random-effect mean  $\kappa$  by color, and each panel corresponds to a different value of the drift function  $\Lambda_i(t, u)$ . These plots demonstrate how the proposed distribution adapts flexibly to different degradation patterns by adjusting the scale and heterogeneity parameters. To further examine the tail behavior, Figure 2(b) compares the proposed distribution with the standard truncated normal and truncated Cauchy distributions, whose tails decay as  $\exp(-y^2)$  and  $y^{-2}$ , respectively. The proposed distribution exhibits a tail decay rate between these two extremes, reflecting a moderate heavy-tail property. As shown in the middle panel ( $y = 4 - 9$ ), the proposed density exceeds that of the truncated normal, allowing it to capture larger degradation values. Beyond this range, it decays faster than the truncated Cauchy, effectively preventing unrealistically large degradation. This balance enables the model to represent occasional large degradation events while maintaining physically reasonable tail behavior for reliability analysis.

### 2.3. Reliability analysis

In engineering applications, predicting a product's failure time is crucial for reliability analysis. We denote the failure threshold by  $\mathcal{H}$ , with the failure time distribution expressed as  $P(T_{\mathcal{H}} < t) = F(\mathcal{Y}(t, u) \geq \mathcal{H})$ . To focus on population-level behavior, we omit the subscript  $i$ . In practice, engineers typically perform periodic inspections based on a product's service age  $t$ , while recording cumulative usage as  $u = \varrho(t)$ , a time-dependent function. This function may be linear, such as  $u = \xi t$ , where  $\xi$  represents a fixed usage rate (Wang et al., 2020). Alternatively,  $\varrho(t)$  can be defined with  $\xi$  as a random variable to capture usage rate variability (Zhai et al., 2023). Specifying  $\varrho(t)$  allows the two-scale degradation model to be reduced to a single-scale form parameterized by  $t$ . Given  $\gamma$ , the conditional cumulative distribution function (CDF) of failure time is:

$$F_{T_{\mathcal{H}}}(t \mid \gamma; \mathcal{H}, \Upsilon(t)) = 1 - \left\{ \Phi \left[ \sqrt{\mathcal{H}}\gamma - \frac{\Upsilon(t)}{\sqrt{\mathcal{H}}} \right] + e^{2\Upsilon(t)\gamma} \Phi \left[ -\sqrt{\mathcal{H}}\gamma - \frac{\Upsilon(t)}{\sqrt{\mathcal{H}}} \right] \right\}, \quad (6)$$

where  $\Upsilon(t) = \Lambda^t(t) + \Lambda^u(\varrho(t))$ . Subsequently, by integrating out  $\gamma$  from (6), Proposition 2 provides the CDF of the unconditional failure time.

**Proposition 2.** *The unconditional failure time distribution is given by*

$$F_{T_{\mathcal{H}}}(t; \mathcal{H}, \Upsilon(t), \kappa, \sigma^2) = 1 - \Phi \left( \frac{-\Upsilon(t)/\sqrt{\mathcal{H}} + \kappa\sqrt{\mathcal{H}}}{\sqrt{1 + \mathcal{H}\sigma^2}} \right) - \exp [2\Upsilon(t)\kappa + 2\Upsilon(t)^2\sigma^2] \times \Phi \left( \frac{-\frac{\Upsilon(t)}{\sqrt{\mathcal{H}}} - \sqrt{\mathcal{H}}\kappa - 2\Upsilon(t)\sqrt{\mathcal{H}}\sigma^2}{\sqrt{1 + \mathcal{H}\sigma^2}} \right). \quad (7)$$

Given (7), the mean-time-to-failure (MTTF) can be computed as:

$$\mathcal{M}T\mathcal{T}\mathcal{F} = \mathbb{E}(T_{\mathcal{H}}) = \int_0^{\infty} 1 - F_{T_{\mathcal{H}}}(t; \Upsilon(t), \kappa, \sigma^2, \mathcal{H}) dt. \quad (8)$$

The proof of (7) is provided in [supplementary Section S1.2](#). It is worth noting that the failure time distribution for models  $M_2$  and  $M_3$  can be derived in a similar manner, as  $\gamma_i$  continues to serve as a random-effects term. In contrast, for models  $M_1$  and  $M_4$ , the failure time distribution corresponds to a standard fixed-effects rIG process, following the structure given in (6).

## 3. Statistical inference

### 3.1. Data and likelihood

Assume that each unit  $i$  is inspected at time points  $\mathbf{t}_i = (t_{i0}, \dots, t_{im_i})'$ , with the corresponding cumulative usage levels recorded as  $\mathbf{u}_i = (u_{i0}, \dots, u_{im_i})'$ . The degradation mea-

surement for unit  $i$  at time  $t_{ij}$  is represented as  $y_{ij}$  for  $i = 1, 2, \dots, n$  and  $j = 0, 1, \dots, m_i$ , with the initial condition  $y_{i0} = 0$  at  $t_{i0} = 0$ . According to model  $[M_0]$ ,  $y_{ij}$  consists of degradation from the age scale,  $x_{ij}$ , and degradation from the usage scale,  $z_{ij}$ . For simplicity, we denote the drift parameters as  $\Lambda_{ij}^t = \Lambda^t(t_{ij}; \alpha_t, \beta_t)$  and  $\Lambda_{ij}^u = \Lambda^u(u_{ij}; \alpha_u, \beta_u)$ , with  $\boldsymbol{\phi}_t = (\alpha_t, \beta_t)'$  and  $\boldsymbol{\phi}_u = (\alpha_u, \beta_u)'$  as the respective parameter vectors.

Define  $\boldsymbol{\Delta y}_i = (\Delta y_{i1}, \dots, \Delta y_{im_i})'$ , where each increment  $\Delta y_{ij} = y_{ij} - y_{i,j-1}$  represents the degradation increments for the  $i$ -th unit at inspection time  $t_{ij}$ . Each  $\Delta y_{ij}$  is composed of increments  $\Delta x_{ij} = x_{ij} - x_{i,j-1}$  and  $\Delta z_{ij} = z_{ij} - z_{i,j-1}$ . Define the vectors  $\boldsymbol{\Delta x}_i = (\Delta x_{i1}, \dots, \Delta x_{im_i})'$  and  $\boldsymbol{\Delta z}_i = (\Delta z_{i1}, \dots, \Delta z_{im_i})'$  to represent these increments. Similarly, let  $\boldsymbol{\Delta \tau}_i = (\Delta \tau_{i1}, \dots, \Delta \tau_{im_i})'$  and  $\boldsymbol{\Delta \nu}_i = (\Delta \nu_{i1}, \dots, \Delta \nu_{im_i})'$ , where  $\Delta \tau_{ij} = \Lambda_{ij}^t - \Lambda_{i,j-1}^t$  and  $\Delta \nu_{ij} = \Lambda_{ij}^u - \Lambda_{i,j-1}^u$  represent the changes in the drift parameters over time. The complete observed data set is denoted by  $\mathbb{Q} = \{\mathbb{Q}_1, \dots, \mathbb{Q}_n\}$ , where  $\mathbb{Q}_i = \{\boldsymbol{\Delta y}_i, \mathbf{t}_i, \mathbf{u}_i\}$ . The model parameter vector is defined as  $\boldsymbol{\Theta} = (\alpha_t, \beta_t, \alpha_u, \beta_u, \kappa, \sigma^2)'$ . Based on Proposition 1, the log-likelihood function is given by

$$\ell(\boldsymbol{\Theta}; \mathbb{Q}) = \sum_{i=1}^n \sum_{j=1}^{m_i} \left[ -\frac{1}{2} \log(2\pi) - \frac{3}{2} \log \Delta y_{ij} - \frac{1}{2} \log(1 + \Delta y_{ij} \sigma^2) + \log(\Delta \tau_{ij} + \Delta \nu_{ij}) - \frac{\kappa^2 \Delta y_{ij} - 2\kappa(\Delta \tau_{ij} + \Delta \nu_{ij}) + (\Delta \tau_{ij} + \Delta \nu_{ij})^2 / \Delta y_{ij}}{2(\Delta y_{ij} \sigma^2 + 1)} \right]. \quad (9)$$

Given the high dimensionality of the parameter vector  $\boldsymbol{\Theta}$ , directly maximizing (9) is challenging. Therefore, we employ two inference methods: an EM algorithm, detailed in Section 3.2, and a Bayesian approach, discussed in [supplementary Section S5](#).

### 3.2. EM algorithm

The EM algorithm iteratively finds ML estimates when latent variables or incomplete data are involved (Wang et al., 2026). Here, we treat  $\boldsymbol{\Delta x} = \{\boldsymbol{\Delta x}_1, \boldsymbol{\Delta x}_2, \dots, \boldsymbol{\Delta x}_n\}$  and  $\boldsymbol{\gamma} = (\gamma_1, \gamma_2, \dots, \gamma_n)'$  as missing data, with  $\{\mathbb{Q}, \boldsymbol{\Delta x}, \boldsymbol{\gamma}\}$  forming the complete dataset. Given that  $\gamma_i \sim \mathcal{N}(\kappa, \sigma^2)$ ,  $\Delta x_{ij} \mid \gamma_i \sim r\mathcal{IG}(\Delta \tau_{ij}, \gamma_i)$ , and  $(\Delta y_{ij} - \Delta x_{ij}) \mid (\Delta x_{ij}, \gamma_i) \sim r\mathcal{IG}(\Delta \nu_{ij}, \gamma_i)$ , the complete log-likelihood function is provided by

$$\ell(\boldsymbol{\Theta}; \mathbb{Q}, \boldsymbol{\Delta x}, \boldsymbol{\gamma}) = \ell(\alpha_u, \beta_u; \mathbb{Q} \mid \boldsymbol{\Delta x}, \boldsymbol{\gamma}) + \ell(\alpha_t, \beta_t; \boldsymbol{\Delta x} \mid \boldsymbol{\gamma}) + \ell(\kappa, \sigma^2; \boldsymbol{\gamma}),$$

where

$$\begin{aligned}
\ell(\alpha_u, \beta_u; \mathbb{Q} \mid \Delta \mathbf{x}, \boldsymbol{\gamma}) &= \sum_{i=1}^n \sum_{j=1}^{m_i} \left[ -\frac{1}{2} \log(2\pi) - \frac{3}{2} [\log(1 - \Delta x_{ij}/\Delta y_{ij}) + \log \Delta y_{ij}] + \log \Delta \nu_{ij} \right. \\
&\quad \left. - \frac{1}{2} \left( \gamma_i \sqrt{\Delta y_{ij} - \Delta x_{ij}} - \Delta \nu_{ij} / \sqrt{\Delta y_{ij} - \Delta x_{ij}} \right)^2 \right], \\
\ell(\alpha_t, \beta_t; \Delta \mathbf{x} \mid \boldsymbol{\gamma}) &= \sum_{i=1}^n \sum_{j=1}^{m_i} \left[ -\frac{1}{2} \log(2\pi) - \frac{3}{2} \log \Delta x_{ij} + \log \Delta \tau_{ij} \right. \\
&\quad \left. - \frac{1}{2} \left( \gamma_i \sqrt{\Delta x_{ij}} - \Delta \tau_{ij} / \sqrt{\Delta x_{ij}} \right)^2 \right], \\
\ell(\kappa, \sigma^2; \boldsymbol{\gamma}) &= \sum_{i=1}^n -\frac{1}{2} [\log(2\pi) + \log \sigma^2 + (\kappa - \gamma_i)^2 / \sigma^2].
\end{aligned}$$

The EM algorithm alternates between the E-step and M-step to iteratively estimate  $\Theta$  until convergence. Starting with the current parameter estimates  $\Theta^{(s)}$  from the  $s$ -th iteration, we define  $\Delta \varsigma_{ij} = \Delta x_{ij} / \Delta y_{ij}$  and calculate the Q-function for the  $(s+1)$ -th iteration as follows:

$$\begin{aligned}
Q(\Theta \mid \Theta^{(s)}) &= \mathbb{E} \left[ \ell(\Theta; \mathbb{Q}, \Delta \mathbf{x}, \boldsymbol{\gamma}) \mid \mathbb{Q}, \Theta^{(s)} \right] \\
&= \sum_{i=1}^n \left\{ -\frac{1}{2} \left( \sum_{j=1}^{m_i} \Delta y_{ij} + \frac{1}{\sigma^2} \right) \mathbb{E}_{\gamma_i \mid \mathbb{Q}_i, \Theta^{(s)}} [\gamma_i^2] + \left[ \sum_{j=1}^{m_i} (\Delta \tau_{ij} + \Delta \nu_{ij}) + \frac{\kappa}{\sigma^2} \right] \mathbb{E}_{\gamma_i \mid \mathbb{Q}_i, \Theta^{(s)}} [\gamma_i] \right. \\
&\quad - \frac{3}{2} \sum_{j=1}^{m_i} \mathbb{E}_{\Delta \varsigma_{ij} \mid \mathbb{Q}_i, \Theta^{(s)}} [\log(1 - \Delta \varsigma_{ij})] - \frac{1}{2} \sum_{j=1}^{m_i} \frac{\Delta \nu_{ij}^2}{\Delta y_{ij}} \mathbb{E}_{\Delta \varsigma_{ij} \mid \mathbb{Q}_i, \Theta^{(s)}} [(1 - \Delta \varsigma_{ij})^{-1}] \\
&\quad \left. - \frac{3}{2} \sum_{j=1}^{m_i} \mathbb{E}_{\Delta \varsigma_{ij} \mid \mathbb{Q}_i, \Theta^{(s)}} [\log(\Delta \varsigma_{ij})] - \frac{1}{2} \sum_{j=1}^{m_i} \frac{\Delta \tau_{ij}^2}{\Delta y_{ij}} \mathbb{E}_{\Delta \varsigma_{ij} \mid \mathbb{Q}_i, \Theta^{(s)}} [\Delta \varsigma_{ij}^{-1}] \right\} + \mathcal{C}_0,
\end{aligned} \tag{10}$$

where  $\mathcal{C}_0 = -(M+n/2) \log(2\pi) + \sum_{i=1}^n \sum_{j=1}^{m_i} [\log(\Delta \nu_{ij} \Delta \tau_{ij}) - 3 \log \Delta y_{ij}] - n \log \sigma - (n\kappa^2)/(2\sigma^2)$ , and  $M = \sum_{i=1}^n m_i$ . The Q-function involves six conditional expectations calculated with respect to the conditional distribution  $f(\Delta \mathbf{x}, \boldsymbol{\gamma} \mid \mathbb{Q}, \Theta^{(s)})$ . These expectations are  $\mathbb{E}_{\gamma_i \mid \mathbb{Q}_i, \Theta^{(s)}} [\gamma_i]$ ,  $\mathbb{E}_{\gamma_i \mid \mathbb{Q}_i, \Theta^{(s)}} [\gamma_i^2]$ ,  $\mathbb{E}_{\Delta \varsigma_{ij} \mid \mathbb{Q}_i, \Theta^{(s)}} [\log(1 - \Delta \varsigma_{ij})]$ ,  $\mathbb{E}_{\Delta \varsigma_{ij} \mid \mathbb{Q}_i, \Theta^{(s)}} [(1 - \Delta \varsigma_{ij})^{-1}]$ ,  $\mathbb{E}_{\Delta \varsigma_{ij} \mid \mathbb{Q}_i, \Theta^{(s)}} [\Delta \varsigma_{ij}^{-1}]$ , and  $\mathbb{E}_{\Delta \varsigma_{ij} \mid \mathbb{Q}_i, \Theta^{(s)}} [\log(\Delta \varsigma_{ij})]$ . We need the following results to derive the conditional expectations.

**Theorem 1.** *Given  $\mathbb{Q}_i, \gamma_i \mid \mathbb{Q}_i \sim \mathcal{N} \left( \frac{\kappa/\sigma^2 + \sum_{j=1}^{m_i} (\Delta \nu_{ij} + \Delta \tau_{ij})}{1/\sigma^2 + \sum_{j=1}^{m_i} \Delta y_{ij}}, \frac{1}{1/\sigma^2 + \sum_{j=1}^{m_i} \Delta y_{ij}} \right)$ . Hence, we have*

$$\begin{aligned}
\mathbb{E}_{\gamma_i \mid \mathbb{Q}_i} [\gamma_i] &= \frac{\kappa/\sigma^2 + \sum_{j=1}^{m_i} (\Delta \nu_{ij} + \Delta \tau_{ij})}{1/\sigma^2 + \sum_{j=1}^{m_i} \Delta y_{ij}}, \\
\mathbb{E}_{\gamma_i \mid \mathbb{Q}_i} [\gamma_i^2] &= \frac{1/\sigma^2 + \sum_{j=1}^{m_i} \Delta y_{ij} + \left( \kappa/\sigma^2 + \sum_{j=1}^{m_i} (\Delta \nu_{ij} + \Delta \tau_{ij}) \right)^2}{\left[ 1/\sigma^2 + \sum_{j=1}^{m_i} \Delta y_{ij} \right]^2}.
\end{aligned} \tag{11}$$

Given  $\mathbb{Q}_i$ , then we have:

$$f(\Delta\varsigma_{ij} | \mathbb{Q}_i) = \frac{(1 - \varsigma_{i,j})^{-3/2} \varsigma_{i,j}^{-3/2} \exp\left[-\frac{1}{2\Delta y_{i,j}} \left(\frac{\Delta\nu_{i,j}^2}{1-\varsigma_{i,j}} + \frac{\Delta\tau_{i,j}^2}{\varsigma_{i,j}}\right)\right]}{\int_0^1 (1 - \varsigma_{i,j})^{-3/2} \varsigma_{i,j}^{-3/2} \exp\left[-\frac{1}{2\Delta y_{i,j}} \left(\frac{\Delta\nu_{i,j}^2}{1-\varsigma_{i,j}} + \frac{\Delta\tau_{i,j}^2}{\varsigma_{i,j}}\right)\right] d\varsigma_{ij}}. \quad (12)$$

We can obtain the remaining four conditional expectations related to the function  $\Delta\varsigma_{ij}$ , i.e.,  $g(\Delta\varsigma_{ij})$ , as follows:

$$\mathbb{E}_{\Delta\varsigma_{ij}|\mathbb{Q}_i, \Theta^{(s)}}[g(\Delta\varsigma_{ij})] = \int_0^1 g(\Delta\varsigma_{ij}) f(\Delta\varsigma_{ij} | \mathbb{Q}_i) d\Delta\varsigma_{ij}. \quad (13)$$

The proof of Theorem 1 is provided in [supplementary Section S2.1](#). To approximate the integral in (13), we present three methods: Trapezoidal approximation (TZ), MC integration, and Gauss-Legendre (GL) quadrature, with detailed theoretical explanations available in [supplementary Section S2.3](#). In Section 4.3, these methods are compared, and we find that the GL quadrature method with an order of  $l = 30$  performs best in balancing efficiency and accuracy. Therefore, this method is adopted to approximate the integral in this study.

Given Theorem 1, the Q-function is fully specified. The optimal solution for the  $(s+1)$ -th iteration in the M-step is updated as:

$$\Theta^{(s+1)} = \arg \max_{\Theta} Q(\Theta | \Theta^{(s)}). \quad (14)$$

This involves computing the partial derivatives of  $Q(\Theta | \Theta^{(s)})$  with respect to each parameter and solving the resulting equations. The parameter update formulas are provided in Theorem 2, with detailed derivations available in [supplementary Section S2.2](#).

**Theorem 2.** Starting from the M-step solution at the  $s$ -th iteration, denoted as  $\Theta^{(s)}$ , the update for (14) in the next iteration is determined as follows:

$$\kappa^{(s+1)} = \frac{\mathbb{E}_{\gamma_i|\mathbb{Q}_i, \Theta^{(s)}}[\gamma_i]}{n}, \text{ and } \sigma^{2(s+1)} = \frac{\sum_{i=1}^n \left( \mathbb{E}_{\gamma_i|\mathbb{Q}_i, \Theta^{(s)}}[\gamma_i^2] - 2\kappa^{(s+1)} \mathbb{E}_{\gamma_i|\mathbb{Q}_i, \Theta^{(s)}}[\gamma_i] \right)}{n} + \kappa^{2(s+1)}.$$

Besides, the update of  $\phi_t^{(s+1)} = (\alpha_t^{(s+1)}, \beta_t^{(s+1)})'$ , and  $\phi_u^{(s+1)} = (\alpha_u^{(s+1)}, \beta_u^{(s+1)})'$  can be implemented by solving the following functions:

$$\begin{aligned} \sum_{i=1}^n \sum_{j=1}^{m_i} \frac{\partial \Delta\tau_{ij}}{\partial \phi_t} \left\{ \mathbb{E}_{\gamma_i|\mathbb{Q}_i, \Theta^{(s)}}[\gamma_i] - \frac{\Delta\tau_{ij}}{\Delta y_{ij}} \mathbb{E}_{\Delta\varsigma_{ij}|\mathbb{Q}_i, \Theta^{(s)}}[\Delta\varsigma_{ij}^{-1}] + \frac{1}{\Delta\tau_{ij}} \right\} &= \mathbf{0}, \\ \sum_{i=1}^n \sum_{j=1}^{m_i} \frac{\partial \Delta\nu_{ij}}{\partial \phi_u} \left\{ \mathbb{E}_{\gamma_i|\mathbb{Q}_i, \Theta^{(s)}}[\gamma_i] - \frac{\Delta\nu_{ij}}{\Delta y_{ij}} \mathbb{E}_{\Delta\varsigma_{ij}|\mathbb{Q}_i, \Theta^{(s)}}[(1 - \Delta\varsigma_{ij})^{-1}] + \frac{1}{\Delta\nu_{ij}} \right\} &= \mathbf{0}. \end{aligned}$$

Given initial values  $\Theta^{(0)}$ , the EM algorithm iterates until a predefined convergence criterion is satisfied. Specifically, convergence is achieved when  $|\Theta^{(s+1)} - \Theta^{(s)}| < \epsilon$ , where  $|\cdot|$  represents the absolute difference and  $\epsilon$  is a preset tolerance. The final parameter estimates are denoted as  $\hat{\Theta}$ . The steps of the EM algorithm used in this study are summarized in Algorithm 1. Details on implementing the EM algorithm for model variants are provided in [supplementary Section S3](#). To improve convergence speed, selecting an effective starting point is crucial. Initial estimates can be obtained by treating each degradation path as an independent instance of a basic nonlinear rIG process. Guidelines for initializing the algorithm are discussed in [supplementary Section S2.4](#).

---

**Algorithm 1:** Implementation of the proposed EM algorithm.

---

**Input:**  $\mathbb{Q}$ ,  $\Theta^{(0)}$ ,  $\epsilon$ .

**Output:**  $\hat{\Theta} = (\hat{\alpha}_t, \hat{\gamma}_t, \hat{\alpha}_u, \hat{\gamma}_u, \hat{\kappa}, \hat{\sigma}^2)'$ .

**while**  $|\Theta^{(s+1)} - \Theta^{(s)}| \geq \epsilon$  **do**

**E-step:**

    Compute  $\mathbb{E}_{\gamma_i|\mathbb{Q}_i, \Theta^{(s)}}[\gamma_i]$ ,  $\mathbb{E}_{\gamma_i|\mathbb{Q}_i, \Theta^{(s)}}[\gamma_i^2]$ , and  $\mathbb{E}_{\Delta\zeta_{ij}|\mathbb{Q}_i, \Theta^{(s)}}[g(\Delta\zeta_{ij})]$  by Theorem 1;

**M-step:**

    Update  $\Theta^{(s+1)}$  by Theorem 2.

**end**

---

### 3.3. Interval estimation

Beyond point estimation, establishing interval estimates for the model parameters  $\Theta$  is essential. These intervals account for uncertainty and variability in the estimates, offering a plausible range for the parameters, which helps practitioners evaluate the precision and reliability of the results (Ouyang et al., 2026). A confidence interval (CI) based on the bootstrap method can be used, as outlined in [Algorithm S1 in supplementary Section S4](#). With  $B$  bootstrap estimates  $\{\hat{\Theta}_1^*, \dots, \hat{\Theta}_B^*\}$  in hand, an approximate  $100(1 - \alpha)\%$  bootstrap CI for a function of the parameters  $h(\Theta)$  can be constructed. This interval is given by:  $[h(\hat{\Theta}^*)_{(\alpha B/2)}, h(\hat{\Theta}^*)_{((1-\alpha/2)B)}]$  where  $h(\hat{\Theta}^*)_{(b)}$  denotes the  $b$ -th order statistic from  $\{h(\hat{\Theta}^*)_1, \dots, h(\hat{\Theta}^*)_B\}$ .

## 4. Simulation studies

To evaluate the proposed methodology, we conduct MC simulations using degradation data generated from model [M<sub>0</sub>]. Both the EM algorithm and Bayesian methods are applied to estimate the model parameters. To examine the effects of sample size and measurement frequency, we consider configurations with  $n = 10, 30, 50$  and  $m = 20, 40$ . The age-scale and usage-scale functions are defined as  $\Lambda^t(t; \alpha_t, \beta_t) = \beta_t t^{\alpha_t}$  and  $\Lambda^u(u; \alpha_u, \beta_u) = \beta_u u^{\alpha_u}$ , respectively. The parameters are set to  $\alpha_t = 1.2$ ,  $\alpha_u = 0.8$ ,  $\beta_t = 4$ ,  $\beta_u = 1$ ,  $\kappa = 5$ , and  $\sigma^2 = 0.5$ .

Degradation values are generated at uniform time intervals  $\Delta t_{ij} = t_{ij} - t_{i,j-1} = 1$ , while the usage scale increment is defined as  $\Delta \varpi_{ij} = \varrho(t_{ij}) - \varrho(t_{i,j-1}) = \xi_j \Delta t_{ij}$ . To reflect stochastic usage patterns observed in practice, the usage rate  $\xi_j$  follows an independent and identically distributed  $r\mathcal{IG}(10, 1)$  distribution. Note that the model does not rely on equally spaced inspections nor on a fixed number of inspection points. Results for irregular inspection schedules are included in the supplementary material. For each configuration, we perform 200 replications, applying both inference methods on a laptop with an Apple M2 Pro CPU. The accuracy of parameter estimation is evaluated by calculating the relative bias (RB) and relative root mean square error (RRMSE) across combinations of  $n$  and  $m$ . These metrics are defined as follows:

$$\text{RB}(\hat{\vartheta}) = \frac{1}{200} \sum_{i=1}^{200} \left( \frac{\hat{\vartheta}_i - \vartheta}{\vartheta} \right), \text{ and } \text{RRMSE}(\hat{\vartheta}) = \left[ \frac{1}{200} \sum_{i=1}^{200} \left( \frac{\hat{\vartheta}_i - \vartheta}{\vartheta} \right)^2 \right]^{1/2},$$

where  $\vartheta$  denotes the true parameter value, and  $\hat{\vartheta}_i$  represents the estimate obtained from the  $i$ -th replication. Smaller values indicate greater estimation accuracy.

### 4.1. Validation of model parameter estimators

For the ML method, point estimates are obtained using the EM algorithm described in Section 3.2. The algorithm iterates until the convergence criterion  $|\Theta^{(s+1)} - \Theta^{(s)}| < 10^{-4}$  is satisfied, typically stabilizing within a reasonable number of iterations. For the Bayesian method, posterior samples of  $\Theta$  are generated via the HMC algorithm (details in [supplementary Section S5](#)). To reflect limited prior knowledge, we adopt weakly informative priors for the Bayesian inference:  $(\kappa, \sigma^2) \sim \text{NIGa}(10, 10^{-6}, 10^{-3}, 10^{-3})$ , and independent normal priors  $\mathcal{N}(1, 10^6)$  for  $(\alpha_t, \alpha_u, \beta_t, \beta_u)$ . Although the normal priors on  $\beta_t$  and  $\beta_u$  assign small probability mass to negative values, our sensitivity analysis using truncated-normal

priors enforcing  $\beta_t, \beta_u > 0$  (reported in supplementary Section S6.4) shows that the posterior estimates are very similar. After a burn-in of  $\mathcal{L} = 1000$  iterations, an additional 4000 iterations are performed to obtain posterior samples, and parameter estimates are calculated as the posterior means of these samples.

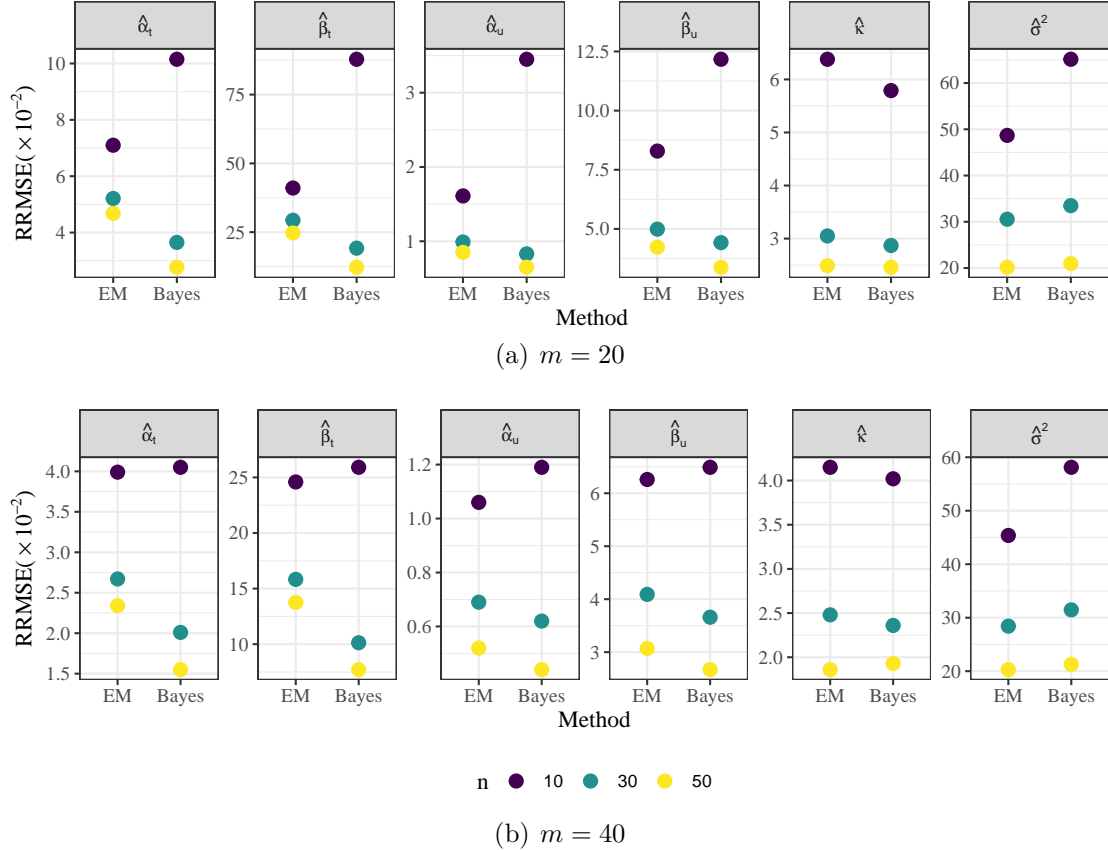


Figure 3: RRMSE of estimates for both methods across various sample sizes and measurement frequencies.

Figure 3 illustrates the RRMSE of parameter estimates across various sample sizes ( $n$ ) and measurement frequencies ( $m$ ) for both inference methods. The results show that RRMSE decreases as  $n$  or  $m$  increases, highlighting that larger samples improve estimation accuracy. Both the Bayesian and EM methods exhibit comparable performance, with similar RRMSE values for most parameters. Notably, as  $n$  increases, more information about the random effects becomes available, significantly enhancing the estimation accuracy of random-effect parameters (e.g.,  $\kappa$  and  $\sigma^2$ ). On the other hand, when  $m$  and  $n$  are relatively small, the accuracy of other parameters is more impacted.

To further evaluate the method, we analyze the influence of degradation curvature ( $\alpha$ )

in the age scale  $t^\alpha$  on estimation performance. One curvature is fixed at 1, while the other varies across 0.7, 1, and 1.3, representing concave, linear, and convex degradation trends, respectively. We also investigate the effects of different degradation scale ratios (smaller, equal, and larger) and sample heterogeneity. In addition, estimation accuracy is assessed across the four model structures  $M_1$ – $M_4$ . These analyses consistently demonstrate that the proposed inference procedures are both reliable and efficient. Furthermore, the interval estimation performance of the Bayesian and bootstrap approaches has also been evaluated through simulation. The Bayesian intervals remain close to the nominal level in small-sample settings, whereas the bootstrap intervals may exhibit slight undercoverage when  $n$  is small. Detailed results are provided in supplementary Section S6.5.

#### 4.2. Validation of reliability estimation

To assess reliability estimation performance, we calculate the MTTF based on the estimated parameters and a failure threshold of 30 (i.e.,  $\mathcal{H} = 30$ ). The MTTF is computed for each simulated sample and compared to the true MTTF. Figure 4 shows box plots of the RRMSE for MTTF estimates across various sample sizes and measurement frequencies. Both inference methods produce MTTF estimates with low RRMSE values, which decrease with larger sample sizes, reducing outliers.

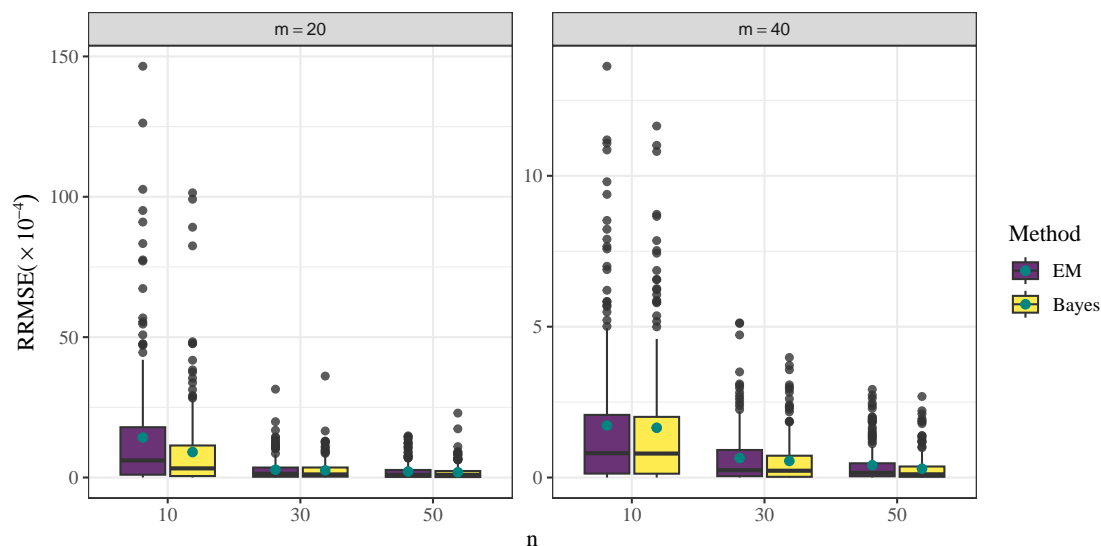


Figure 4: RRMSE of MTTF estimators for different sample sizes and measurement frequencies (green points indicate average RRMSEs).

Additionally, we evaluate the effect of model misspecification on reliability estimates.

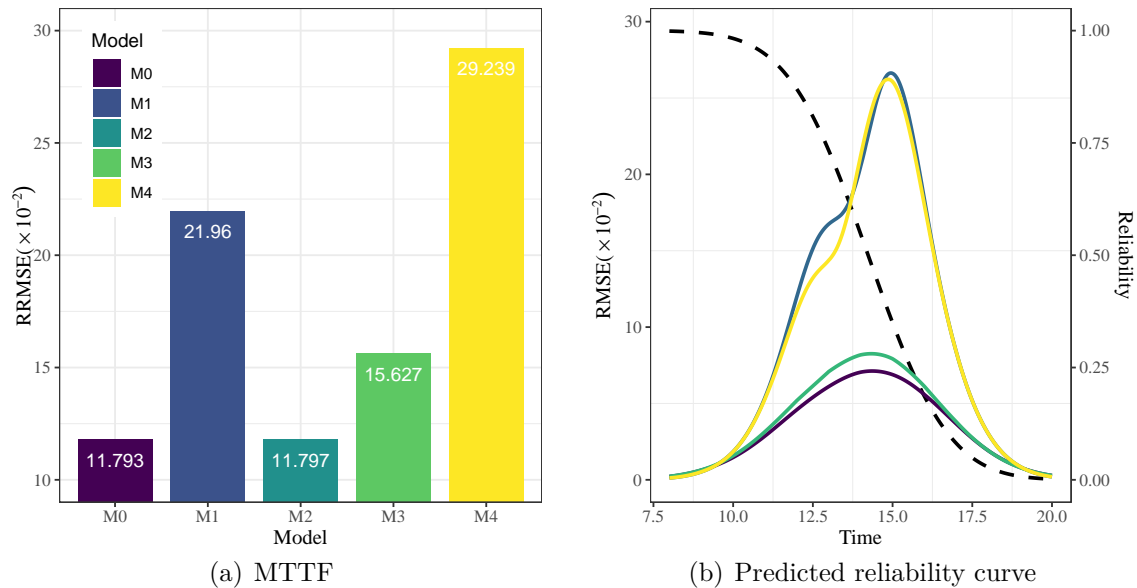


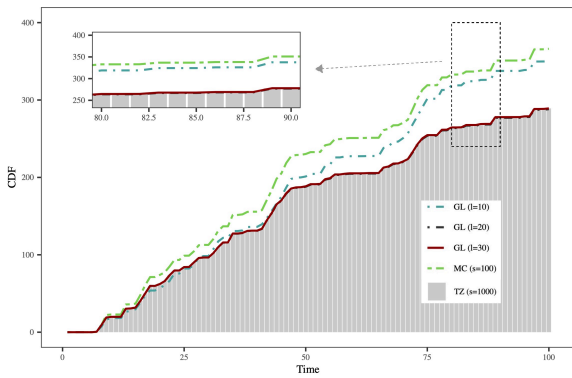
Figure 5: Reliability evaluation of different models, including (a) the comparison of MTTF prediction errors and (b) the predicted reliability curves over time.

Using the parameter settings in Section 4, simulated data are generated, and different models are applied for parameter estimation. Reliability at various time points is calculated for each model and compared to the true reliability. Figure 5(a) presents the RRMSE of MTTF estimates across 200 simulations ( $n = 10$  and  $m = 30$ ), while Figure 5(b) illustrates the corresponding reliability performance, with the black dashed line representing the true reliability curve. Since RRMSE may be undefined when values are zero, RMSE is used as an alternative metric here.

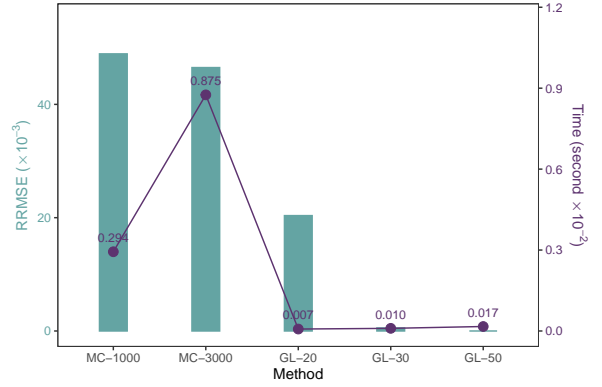
The figures demonstrate the importance of properly handling random effects and scales for accurate reliability estimation. Specifically, two-scale random effects models (e.g.,  $M_0$  and  $M_2$ ) achieve lower RRMSE values and align more closely with the true reliability curve, indicating that incorporating random effects enhances estimation accuracy when such effects are present in the data. Conversely, fixed effects models (e.g.,  $M_1$  and  $M_4$ ) yield higher estimation errors, underscoring the limitations of ignoring random effects. In terms of scale consideration, two-scale models (e.g.,  $M_0$  and  $M_1$ ) outperform single-scale models (e.g.,  $M_3$  and  $M_4$ ), as single-scale models lack the capacity to capture the complexity inherent in multi-scale degradation, resulting in greater bias in reliability estimates. Thus, accurately modeling two-scale random effects is essential for enhancing the precision of reliability predictions.

### 4.3. Performance of integral approximation methods

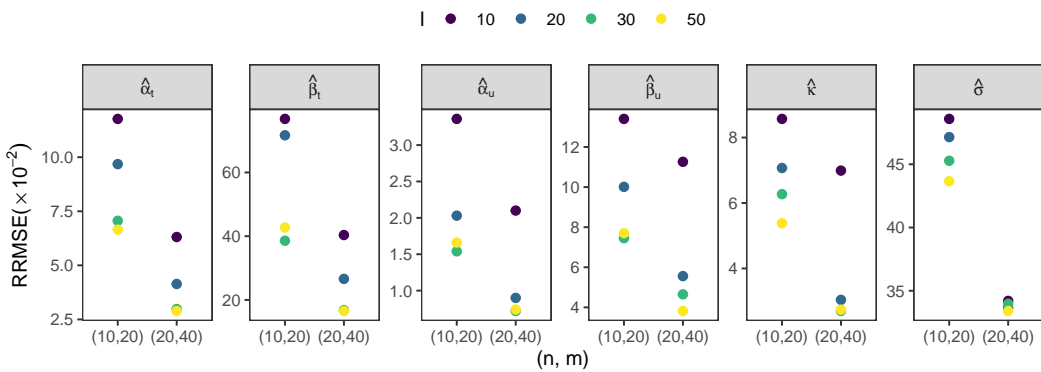
In this section, we evaluate the accuracy and efficiency of different approximation methods using (12) as an example, with a focus on  $f(\Delta\varsigma_{ij} = 0.3 \mid \mathbb{Q}_1)$ , where the denominator involves an expectation over  $\Delta\varsigma_{ij}$ . Figure 6(a) shows the empirical PDF along with results from different approximation methods. The results show that the GL method with  $l = 20$  and  $l = 30$  closely matches the TZ method, which divides the interval  $[0, 1]$  into 1000 subintervals and serves as a near-exact benchmark. However, the GL method at  $l = 10$  performs poorly, and the MC method exhibits even lower accuracy. Using the TZ approximation as a reference, we compute the RRMSE and average computation time for each method (see Figure 6(b)). The GL method demonstrates higher efficiency compared to the MC method, achieving similar accuracy to the TZ method at  $l = 30$  and  $l = 50$ .



(a) Empirical CDF of the conditional distribution



(b) Computation and performance



(c) Performance of EM algorithm

Figure 6: Comparison of different approximation methods in terms of fitting accuracy and computational efficiency, including (a) empirical CDFs of the conditional distribution, (b) the trade-off between computation time and accuracy, and (c) EM algorithm performance for parameter estimation.

We further apply the GL method with varying values of  $l$  in the E-step of the EM algorithm, specifically to compute  $\mathbb{E}_{\Delta\varsigma_{ij}|\mathbb{Q}_i, \Theta^{(s)}}[g(ij)]$ . Through 100 simulations, we compare parameter estimates with true values, with RRMSE results shown in Figure 6(c) for different sample sizes. The findings indicate that as  $l$  increases, the performance of the EM algorithm improves. For  $(n, m) = (10, 20)$ , the runtime for a single EM iteration with  $l = 10, 20, 30, 50$  is 10.66, 53.93, 95.72, and 159.35 seconds respectively. Although the EM algorithm converges quickly with  $l = 10$ , it yields lower predictive accuracy. In contrast,  $l = 30$  achieves nearly the same accuracy as  $l = 50$  while reducing computation time by nearly half. Therefore, to balance accuracy and efficiency, we adopt the GL method with  $l = 30$  for approximating the complex integral in this study.

## 5. Case study

In this section, we illustrate the implementation of the proposed methodology by analyzing the coating material degradation dataset as shown in Figure 1. We begin by fitting the dataset using model  $M_0$  and its variants, where the two drift components follow the power-law forms  $\Lambda^t(t) = \beta_t t^{\alpha_t}$  and  $\Lambda^u(u) = \beta_u u^{\alpha_u}$ . Statistical inference is performed using the corresponding EM or ML methods. Model convergence is evaluated through parameter estimate trajectories, as shown in Figure 7. This figure illustrates the iteration process of the EM algorithm for  $M_0$ , demonstrating that each parameter converges after a sufficient number of iterations. Similar convergence behavior for other models can be found in [supplementary Section S7](#). Although Bayesian methods can also be applied for parameter estimation, they are not included here as they yield comparable results.

To further evaluate the practical value of the proposed two-scale rIG model, we also include several representative baseline models for comparison. (i) A single-scale reparameterized gamma process (RGa) ([Zhou et al., 2023](#)), which employs a linear drift function and introduces unit-specific random effects on the drift rate through a gamma distribution. In our analysis, this model is applied separately to the time and UV scales, denoted  $\text{RGa}(t)$  and  $\text{RGa}(u)$ . (ii) A two-independent-scale gamma model (2IS-Ga), in which degradation is modeled as the sum of two independent gamma processes corresponding to the time and UV scales. Each process adopts the same power-law drift structure as in our formulation and both share a common shape parameter to ensure comparability across scales. All baseline models are estimated using the EM algorithm.

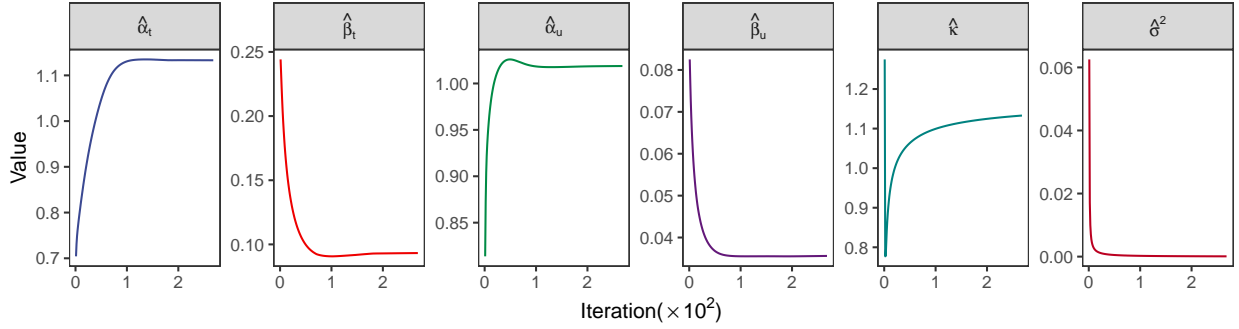


Figure 7: Iteration process of EM algorithm for parameters under model  $M_0$ .

### 5.1. Model fitting and comparison

Table 3: Parameter point estimates regarding the coating material data.

Type	Model	$\alpha_t$	$\beta_t$	$\alpha_u$	$\beta_u$	$\gamma$	$\kappa$	$\sigma$	Loglik	AIC
Two-scale	$M_0$	1.133	0.093	1.019	0.036	—	1.133	0.010	-262.799	537.598
	$M_1$	1.137	0.091	1.018	0.037	1.191	—	—	-262.573	<b>535.146</b>
	$M_2$	1.137	0.091	1.018	0.037	—	1.190	0.013	-262.589	537.178
Single-scale	$M_3(t)$	1.010	0.057	—	—	—	1.193	0.016	-310.149	628.298
	$M_3(u)$	—	—	1.111	0.247	—	0.917	0.037	-278.794	565.588
	$M_4(t)$	1.086	0.277	—	—	0.912	—	—	-309.690	625.380
	$M_4(u)$	—	—	0.980	0.070	1.171	—	—	-278.108	562.216

Table 4: AIC comparison of candidate models.

Model	Two-scale				Single-scale	
	$M_0$	$M_1$	$M_2$	2IS-Ga	RGa( $t$ )	RGa( $u$ )
AIC	537.60	<b>535.15</b>	537.18	535.52	577.02	597.63

Tables 3-4 summarize the parameter estimates, log-likelihood values, and AIC results for all candidate models. For each specification, the log-likelihood is computed by substituting the fitted parameters into (9), and the AIC is obtained as  $\text{AIC} = 2\zeta - 2\ell$ , where  $\ell$  and  $\zeta$  denote the log-likelihood and the number of parameters, respectively. Among all

models,  $M_1$  attains the lowest AIC, indicating the best overall fit for the coating dataset. The 2IS-Ga model produces an AIC value very close to that of  $M_1$ , largely because both models employ a two-scale power-law drift structure and therefore reproduce the global degradation trend similarly well. The key difference lies in their assumed increment distributions: 2IS-Ga imposes gamma-distributed increments with relatively light tails, whereas the proposed two-scale rIG process allows for heavier-tailed variation, which better reflects the local fluctuations observed in the coating data. For the random-effects models  $M_0$  and  $M_2$ , the estimated values of  $\sigma$  are near zero, suggesting limited between-sample heterogeneity and supporting the simpler fixed-effect formulation adopted in  $M_1$ . In comparison, all single-scale models exhibit substantially larger AIC values, as modeling only the time or the UV scale is insufficient to capture their joint influence. The RGa( $t$ ) and RGa( $u$ ) models, which assume a linear drift form, perform even less favorably for this dataset.

The parameter estimates from the selected model  $M_1$  provide interpretable insights into the coating degradation mechanism. The time-scale parameters ( $\alpha_t, \beta_t$ ) characterize calendar-time aging (e.g., oxidation and gradual chain scission), with  $\alpha_t = 1.137$  indicating mildly accelerating degradation over time. Although the UV-scale parameters ( $\alpha_u, \beta_u$ ) are numerically smaller, this does not imply a weaker UV effect. In this experiment, the accumulated UV dose grows much faster than calendar time (e.g., when  $t = 1$ , the corresponding UV dose can already be on the order of several hundred units), so the UV-driven drift  $\beta_u u^{\alpha_u}$  dominates  $\beta_t t^{\alpha_t}$ . This is consistent with established photo-oxidation mechanisms and is visually supported by the two-scale decomposition in Figure 9. To quantify estimation uncertainty for  $M_1$ , we report percentile bootstrap 95% CIs based on 500 resamples:  $\alpha_t \in [0.761, 1.263]$ ,  $\beta_t \in [0.052, 0.220]$ ,  $\alpha_u \in [0.945, 1.136]$ ,  $\beta_u \in [0.017, 0.062]$ , and  $\gamma \in [1.066, 1.360]$ . Under the two-scale decomposition, we can also examine the empirical dependence between the estimated time-driven and UV-driven components. Although both time and UV exposure contribute to degradation, the estimated cross-scale dependence is very small (near zero). This is plausible because calendar-time aging reflects slow, relatively uniform chemical oxidation and structural relaxation, whereas UV-induced degradation is driven primarily by the externally applied UV dose, which increases deterministically with the exposure schedule and is unrelated to the specimen’s intrinsic aging state.

## 5.2. Model adequacy assessment

To assess whether the selected model provides an adequate fit to the coating degradation data, we conduct increment-level goodness-of-fit diagnostics based on probability integral transform (PIT) principles. Specifically, for each observed degradation increment, we evaluate its consistency with the model-implied conditional distribution under the selected model  $M_1$ . Figure 8(a) presents the Uniform Q–Q plot of the PIT values constructed from the fitted two-scale rIG model. Most points closely follow the reference line over the central range, indicating that the model provides an adequate description of the distributional behavior of the degradation increments. Mild deviations are observed near the lower tail, suggesting slight local discrepancies for a small subset of increments, but no systematic lack-of-fit pattern is evident. Figure 8(b) further reports the histogram of the PIT values. The distribution is broadly consistent with a Uniform(0, 1) shape, reinforcing the conclusion that the assumed power-law drift functions capture the primary degradation dynamics in the coating data.

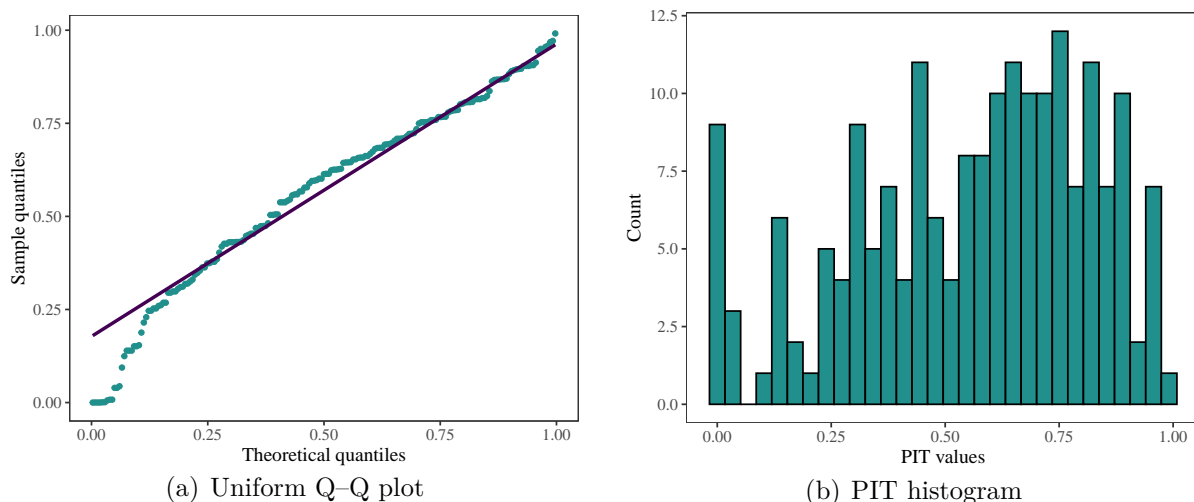


Figure 8: Increment-level goodness-of-fit diagnostics based on PIT under the selected model  $M_1$ : (a) Uniform Q–Q plot of PIT values; (b) histogram of PIT values.

Figure 9 presents the fitted degradation results for groups G9 and G15 under the proposed two-scale model. The black dots represent the observed degradation values, while the red solid curve shows the fitted overall degradation path  $\hat{Y}(t)$  with its 90% confidence band constructed from 500 bootstrap replications (gray shading). The plot also decomposes the degradation into its two components: the time-driven part  $\hat{X}(t)$  (teal dashed line) and the

UV-driven part  $\hat{Z}(u)$  (purple dotted line), illustrating how the two scales jointly contribute to the overall deterioration. As shown in the figure, the component  $\hat{X}(t)$  grows slowly and approximately linearly, reflecting gradual calendar-time aging mechanisms such as thermal oxidation or structural relaxation in polymer coatings. In contrast,  $\hat{Z}(u)$  increases much more rapidly, capturing UV-induced photochemical degradation (e.g., photo-oxidation or chain scission), which dominates the accelerated deterioration observed in the data. The sum of the two components yields the overall path  $\hat{Y}(t)$ , which closely matches the observed trajectories. In addition, the 90% confidence band provides adequate coverage for most units, indicating that the proposed two-scale model effectively captures the physical degradation mechanisms of coating materials under outdoor exposure.

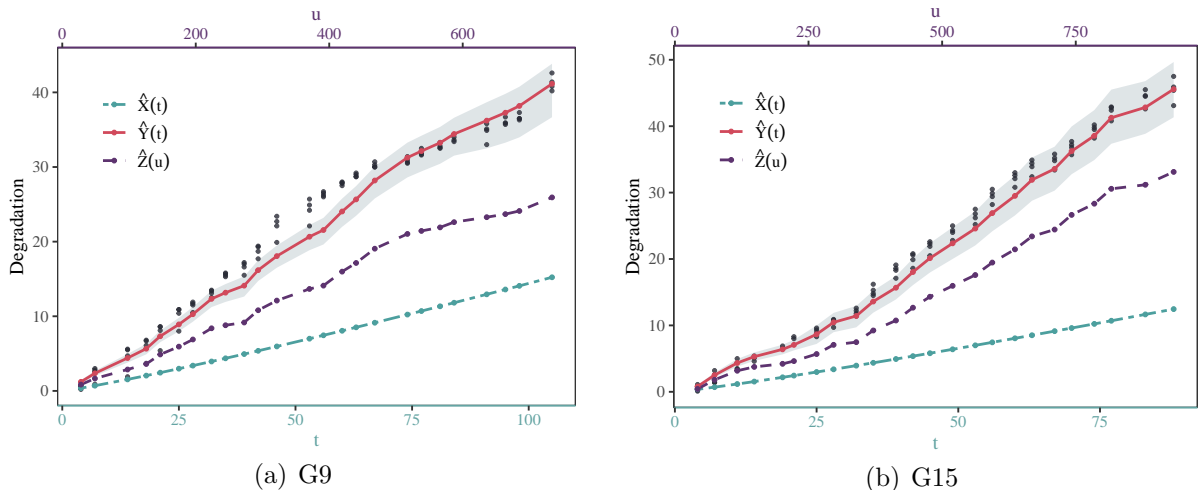


Figure 9: Two-scale decomposition of degradation for groups G9 and G15. Black points show observed values, the red curve is the fitted degradation path with its 90% confidence band, and the teal and purple curves represent the time- and UV-driven components.

### 5.3. Reliability analysis

According to [Hong et al. \(2015\)](#); [Zhai et al. \(2023\)](#), the failure threshold for this coating material is  $\mathcal{H} = 40$ . As shown in Figure 1(b), all units fail within  $t = 100$ , as their degradation values exceed this threshold. Although the exact failure times are not known, we can identify the failure intervals and estimate the failure times using linear interpolation. Assuming the degradation value at time  $t_i$  is  $y_i$  and at time  $t_{i+1}$  is  $y_{i+1}$ , where  $y_i < \mathcal{H}$  and

$y_{i+1} > \mathcal{H}$ , the interpolated failure time  $t_{\mathcal{H}}$  can be calculated as:

$$t_{\mathcal{H}} = t_i + \frac{\mathcal{H} - y_i}{y_{i+1} - y_i} \times (t_{i+1} - t_i). \quad (15)$$

According to the top-to-bottom order in Figure 9, the estimated failure times for the four products in group G9 are 97.84, 97.31, 97.14, and 96.76, and in group G15 are 72.77, 69.76, 70.69, and 70.26.

Using the estimated failure times for each unit, we analyze the reliability predictions across different models. Since the results for G9 are similar to those for G15, we use G15 as an example here. Figure 10(a) shows the reliability curves for the G15-11 coating material under various models, while Figure 10(b) compares the average RRMSE of four units with their estimated failure times calculated by (15), where error bars represent RRMSE deviations. The results indicate that models incorporating both time and UV exposure provide a more accurate depiction of the degradation process. Two-scale models ( $M_0$ ,  $M_1$ , and  $M_2$ ) capture the combined effects of time and UV exposure, leading to lower prediction errors and improved accuracy. In contrast, single-scale models, particularly calendar-time-based ones ( $M_3/M_4$  with time), tend to overestimate reliability, resulting in overly optimistic lifespan predictions. Thus, relying solely on a single degradation scale could misjudge material reliability and increase the risk of premature failure in high-UV environments.

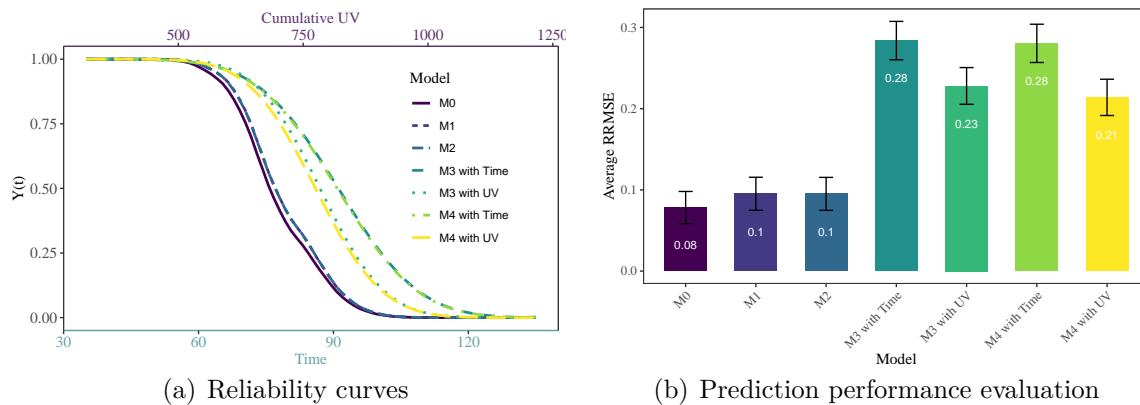


Figure 10: Reliability curves and prediction performance comparison with estimated failure times for the G15 coating material under different models.

## 6. Conclusion and discussion

In this study, we propose a novel two-scale rIG process model specifically designed for products with monotonic degradation paths. Based on physical mechanisms, the model inte-

grates two independent degradation scales—age and usage—allowing it to more accurately describe degradation processes influenced by both time and operational demands. Additionally, we introduce heterogeneity by assigning unique model parameters to each unit, capturing differences between products. The model provides an explicit expression for failure time and describes its corresponding properties. We propose two statistical inference methods: an ML-based approach with bootstrap intervals and a Bayesian approach using HMC sampling. These two strategies are complementary: the ML procedure is computationally efficient and provides reliable point estimates, whereas the Bayesian method offers uncertainty quantification and typically yields more stable interval estimates, especially in small-sample or higher-noise settings. This dual implementation allows practitioners to balance computational cost and uncertainty quantification according to the application context. Comprehensive simulations demonstrate the practical effectiveness of the proposed model. Key findings include: a) Increasing the sample size significantly improves the accuracy of point estimates, yielding more precise parameter values; b) The proposed estimation methods consistently produce reliable results across different settings, including changes in degradation curvature, degradation scale ratios, and sample heterogeneity; c) Ignoring either scale or random effects introduces substantial bias in MTTF estimates. Finally, we illustrate the practical applicability of the proposed approach through a case study. Note that this generalized model framework includes a range of specific variants. To improve accessibility and usability, we develop an R package incorporating the proposed model and its extensions.

While the proposed framework effectively captures two-scale monotonic degradation, several limitations and extensions deserve further investigation. First, the model assumes an additive structure over time and usage. In some systems, cross-scale interactions may be more complex, including nonlinear coupling or compensatory effects (e.g., intensive usage triggering more frequent maintenance and partially offsetting time-driven aging). Capturing such behaviors requires relaxing the additive assumption, for example via an interaction-augmented drift specification  $\Lambda(t, u) = \Lambda^t(t) + \Lambda^u(u) + \beta_{tu}g(t, u)$  with  $g(t, u) = t^{\alpha_t}u^{\alpha_u}$ , or a link-based additive formulation  $h(\mathcal{Y}_i(t, u)) = \mathcal{X}_i(t) + \mathcal{Z}_i(u)$ , where  $h(\cdot)$  is a monotone invertible link (e.g., log or Box–Cox). While these extensions increase structural flexibility, they fundamentally alter the stochastic representation of degradation by breaking additivity and conditional independence. As a result, the rIG closure is lost, likelihood evaluation becomes more involved, and inference typically relies on numerical integration or simulation-based

methods rather than closed-form expressions (Wang et al., 2025; Cao et al., 2025). Second, the baseline model uses a shared random effect for the time- and usage-driven components. Allowing separate (possibly correlated) random effects provides a more granular representation of heterogeneity across degradation channels. However, the primary challenge here is not only computational complexity, but also statistical identifiability. Distinguishing multiple sources of heterogeneity requires sufficient non-collinear variation in the  $(t, u)$  design; otherwise, channel-specific random effects may be weakly identified or confounded with scale-specific drift parameters. In such cases, inference becomes sensitive to prior specification and typically necessitates fully Bayesian sampling strategies or carefully designed experiments. Third, from a practical standpoint, future work may extend the framework to more heterogeneous datasets and additional reliability settings, such as competing risks, time-varying covariates, or reliability-driven decisions including maintenance optimization and warranty planning. The accompanying R package provides a modular basis for such extensions.

### Data availability statement

The coating material degradation data that support the findings of this study are openly available in Gu et al. (2009).

### Acknowledgments

The research is supported by National Natural Science Foundation of China (72571246, 72471119, 72201242), Zhejiang Provincial Natural Science Foundation of China (LZ24A010002, LQK26A010003), the Fundamental Research Funds for the Provincial Universities of Zhejiang (2025ZDAPY01), the Summit Advancement Disciplines of Zhejiang Province (Zhejiang Gongshang University—Statistics), and Collaborative Innovation Center of Statistical Data Engineering Technology & Application.

### Supplementary materials

**Supplementary document:** (S1) Proof of propositions; (S2) Technical details of the EM algorithm, covering conditional expectations, first-order partial derivatives of the Q-function, integral approximation methods, and initial parameter estimates; (S3) Statistical inference for model extensions; (S4) Technical details of the bootstrap method; (S5) Bayesian

inference, including Bayesian formulation and Gibbs and HMC sampling algorithms; (S6) and (S7) Additional simulation experiments and case study. **Source Codes:** the R codes for this paper are provided.

## References

- Asgari, A., Si, W., Yuan, L., Krishnan, K., Wei, W., 2024. Multivariable degradation modeling and life prediction using multivariate fractional Brownian motion. *Reliability Engineering & System Safety* 248, 110146. doi:[10.1016/j.ress.2024.110146](https://doi.org/10.1016/j.ress.2024.110146).
- Barui, S., Mitra, D., Balakrishnan, N., 2024. Flexible modelling of a bivariate degradation process with a shared frailty and an application to fatigue crack data. *Reliability Engineering & System Safety* 242, 109722. doi:[10.1016/j.ress.2023.109722](https://doi.org/10.1016/j.ress.2023.109722).
- Cao, X., Wang, S., Zhou, Y., 2025. glabcmcmc: a Python package for ABC-MCMC with local and global moves. *Statistical Theory and Related Fields* 9, 168–177. doi:[10.1080/24754269.2025.2495505](https://doi.org/10.1080/24754269.2025.2495505).
- Fan, T.H., Dong, Y.S., Peng, C.Y., 2023. A complete Bayesian degradation analysis based on inverse gaussian processes. *IEEE Transactions on Reliability* 73, 536–548. doi:[10.1109/TR.2023.3304673](https://doi.org/10.1109/TR.2023.3304673).
- Fang, G., Pan, R., 2024. A class of hierarchical multivariate wiener processes for modeling dependent degradation data. *Technometrics* 66, 141–156. doi:[10.1080/00401706.2023.2242413](https://doi.org/10.1080/00401706.2023.2242413).
- Fang, G., Pan, R., Wang, Y., 2022. Inverse Gaussian processes with correlated random effects for multivariate degradation modeling. *European Journal of Operational Research* 300, 1177–1193. doi:[10.1016/j.ejor.2021.10.049](https://doi.org/10.1016/j.ejor.2021.10.049).
- Gu, X., Stanley, D., Byrd, W.E., Dickens, B., Vaca-Trigo, I., Meeker, W.Q., Nguyen, T., Chin, J.W., Martin, J.W., 2009. Linking accelerated laboratory test with outdoor performance results for a model epoxy coating system, in: *Service Life Prediction of Polymeric Materials: Global Perspectives*, Springer. pp. 3–28.
- Hong, Y., Duan, Y., Meeker, W.Q., Stanley, D.L., Gu, X., 2015. Statistical methods for degradation data with dynamic covariates information and an application to outdoor weathering data. *Technometrics* 57, 180–193. doi:[10.1080/00401706.2014.915891](https://doi.org/10.1080/00401706.2014.915891).
- Hu, J., Sun, Q., Ye, Z.S., Zhou, Q., 2020. Joint modeling of degradation and lifetime data for RUL prediction of deteriorating products. *IEEE Transactions on Industrial Informatics* 17, 4521–4531. doi:[10.1109/TII.2020.3021054](https://doi.org/10.1109/TII.2020.3021054).
- Li, Q., Li, H., Ma, Z., Liu, X., Guan, X., Zhang, X., 2023. Remaining useful life prediction of mechanical system based on improved adaptive fractional lévy stable motion with statistical dependence measurement error. *Mechanical Systems and Signal Processing* 200, 110646. doi:[10.1016/j.ymsp.2023.110646](https://doi.org/10.1016/j.ymsp.2023.110646).
- Lin, C.P., Ling, M.H., Cabrera, J., Yang, F., Yu, D.Y.W., Tsui, K.L., 2021. Prognostics for lithium-ion batteries using a two-phase gamma degradation process model. *Reliability Engineering & System Safety* 214, 107797. doi:[10.1016/j.ress.2021.107797](https://doi.org/10.1016/j.ress.2021.107797).
- Ling, M.H., Ng, H.K.T., Tsui, K.L., 2019. Bayesian and likelihood inferences on remaining useful life in two-phase degradation models under gamma process. *Reliability Engineering & System Safety* 184, 77–85. doi:[10.1016/j.ress.2017.11.017](https://doi.org/10.1016/j.ress.2017.11.017).

- Liu, H., Song, W., Zio, E., 2022. Fractional lévy stable motion with LRD for RUL and reliability analysis of li-ion battery. *ISA transactions* 125, 360–370. doi:[10.1016/j.isatra.2021.07.002](https://doi.org/10.1016/j.isatra.2021.07.002).
- Lu, L., Wang, B., Hong, Y., Ye, Z., 2020. General path models for degradation data with multiple characteristics and covariates. *Technometrics* 63, 354–369. doi:[10.1080/00401706.2020.1796814](https://doi.org/10.1080/00401706.2020.1796814).
- Ouyang, L., Yan, L., Liu, L., Sun, M., Wang, M., 2026. Double-robust Bayesian variable selection and model prediction with spherically symmetric error. *IISE Transactions* 58, 181–194. doi:[10.1080/24725854.2025.2491492](https://doi.org/10.1080/24725854.2025.2491492).
- Pei, H., Hu, C., Si, X., Zheng, J., Zhang, Q., Zhang, Z., Pang, Z., 2019. Remaining useful life prediction for nonlinear degraded equipment with bivariate time scales. *IEEE Access* 7, 165166–165180. doi:[10.1109/ACCESS.2019.2951804](https://doi.org/10.1109/ACCESS.2019.2951804).
- Peng, C.Y., 2015. Inverse Gaussian processes with random effects and explanatory variables for degradation data. *Technometrics* 57, 100–111. doi:[10.1080/00401706.2013.879077](https://doi.org/10.1080/00401706.2013.879077).
- Peng, C.Y., Cheng, Y.S., 2020. Student-t processes for degradation analysis. *Technometrics* 62, 223–235. doi:[10.1080/00401706.2019.1630008](https://doi.org/10.1080/00401706.2019.1630008).
- Peng, S., Jiang, W., Huang, W., Luo, Q., 2024. The impact of gamma usage processes on preventive maintenance policies under two-dimensional warranty. *Reliability Engineering & System Safety* 242, 109743. doi:[10.1016/j.ress.2023.109743](https://doi.org/10.1016/j.ress.2023.109743).
- Peng, W., Li, Y.F., Yang, Y.J., Huang, H.Z., Zuo, M.J., 2014. Inverse Gaussian process models for degradation analysis: A Bayesian perspective. *Reliability Engineering & System Safety* 130, 175–189. doi:[10.1016/j.ress.2014.06.005](https://doi.org/10.1016/j.ress.2014.06.005).
- Si, X.S., Wang, W., Chen, M.Y., Hu, C.H., Zhou, D.H., 2013. A degradation path-dependent approach for remaining useful life estimation with an exact and closed-form solution. *European Journal of Operational Research* 226, 53–66. doi:[10.1016/j.ejor.2012.10.030](https://doi.org/10.1016/j.ejor.2012.10.030).
- Song, K., Cui, L., 2022. A common random effect induced bivariate gamma degradation process with application to remaining useful life prediction. *Reliability Engineering & System Safety* 219, 108200. doi:[10.1016/j.ress.2021.108200](https://doi.org/10.1016/j.ress.2021.108200).
- Wang, C., Liu, J., Yang, Q., Hu, Q., Yu, D., 2023a. Recoverability effects on reliability assessment for accelerated degradation testing. *IISE Transactions* 55, 698–710. doi:[10.1080/24725854.2022.2089784](https://doi.org/10.1080/24725854.2022.2089784).
- Wang, P., Tang, Y., 2025. Remaining useful life prediction based on exponential dispersion process with random drifts. *Statistical Theory and Related Fields* 9, 404–433. doi:[10.1080/24754269.2025.2555043](https://doi.org/10.1080/24754269.2025.2555043).
- Wang, P., Zhao, W., Tang, Y., 2025. Approximate Bayesian inference based on INLA algorithm. *Statistical Theory and Related Fields* doi:[10.1080/24754269.2025.2588859](https://doi.org/10.1080/24754269.2025.2588859).
- Wang, W., Wang, Y., Zhao, X., 2026. Estimation and inference for fixed center effects on panel count data settings. *Statistical Papers* doi:[10.1007/s00362-026-01807-0](https://doi.org/10.1007/s00362-026-01807-0).
- Wang, X., Li, L., Xie, M., 2020. An unpunctual preventive maintenance policy under two-dimensional warranty. *European Journal of Operational Research* 282, 304–318. doi:[10.1016/j.ejor.2019.09.025](https://doi.org/10.1016/j.ejor.2019.09.025).
- Wang, X., Wang, B.X., Hong, Y., Jiang, P.H., 2021. Degradation data analysis based on gamma process with random effects. *European Journal of Operational Research* 292, 1200–1208. doi:[10.1016/j.ejor.2020.11.036](https://doi.org/10.1016/j.ejor.2020.11.036).
- Wang, X., Xu, D., 2010. An inverse Gaussian process model for degradation data. *Technometrics* 52,

- 188–197. doi:[10.1198/TECH.2009.08197](https://doi.org/10.1198/TECH.2009.08197).
- Wang, X.L., 2023. Design and pricing of usage-driven customized two-dimensional extended warranty menus. *IIESE Transactions* 55, 873–885. doi:[10.1080/24725854.2022.2104972](https://doi.org/10.1080/24725854.2022.2104972).
- Wang, Z., Zhai, Q., Shen, L., 2023b. Degradation modeling and RUL prediction in dynamic environments using a Wiener process with an autoregressive rate. *IEEE Transactions on Reliability* 73, 912–921. doi:[10.1109/TR.2023.3319497](https://doi.org/10.1109/TR.2023.3319497).
- Xu, A., Fang, G., Zhuang, L., Gu, C., 2025. A multivariate student-t process model for dependent tail-weighted degradation data. *IIESE Transactions* 57, 1071–1087. doi:[10.1080/24725854.2024.2389538](https://doi.org/10.1080/24725854.2024.2389538).
- Xu, A., Wang, W., 2025. Recursive Bayesian prediction of remaining useful life for gamma degradation process under conjugate priors. *Scandinavian Journal of Statistics* doi:[10.1111/sjos.70031](https://doi.org/10.1111/sjos.70031).
- Ye, Z.S., Chen, N., 2014. The inverse Gaussian process as a degradation model. *Technometrics* 56, 302–311. doi:[10.1080/00401706.2013.830074](https://doi.org/10.1080/00401706.2013.830074).
- Zhai, Q., Li, Y., Chen, P., 2025. Modeling product degradation with heterogeneity: A general random-effects Wiener process approach. *IIESE Transactions* 57, 1422–1435. doi:[10.1080/24725854.2024.2434125](https://doi.org/10.1080/24725854.2024.2434125).
- Zhai, Q., Xu, A., Yang, J., Zhou, Y., 2023. Statistical modeling and reliability analysis for degradation processes indexed by two scales. *IEEE Transactions on Industrial Informatics* 20, 3675–3684. doi:[10.1109/TII.2023.3313668](https://doi.org/10.1109/TII.2023.3313668).
- Zhang, H., Chen, M., Shang, J., Yang, C., Sun, Y., 2021. Stochastic process-based degradation modeling and RUL prediction: from Brownian motion to fractional Brownian motion. *Science China Information Sciences* 64, 171201. doi:[10.1007/s11432-020-3134-8](https://doi.org/10.1007/s11432-020-3134-8).
- Zhang, Z., Hu, C., Si, X., Zhang, W., 2017. Degradation modeling and remaining useful life prediction with bivariate time scale. *Zidonghua Xuebao/Acta Automatica Sinica* 43, 1789–98. doi:[10.16383/j.aas.2017.c160509](https://doi.org/10.16383/j.aas.2017.c160509).
- Zhang, Z., Si, X., Hu, C., Lei, Y., 2018. Degradation data analysis and remaining useful life estimation: A review on Wiener-process-based methods. *European Journal of Operational Research* 271, 775–796. doi:[10.1016/j.ejor.2018.02.033](https://doi.org/10.1016/j.ejor.2018.02.033).
- Zhao, X., Chen, P., Tang, L.C., 2025. Condition-based maintenance via Markov decision processes: A review. *Frontiers of Engineering Management* 12, 330–342. doi:[10.1007/s42524-024-4130-7](https://doi.org/10.1007/s42524-024-4130-7).
- Zhou, S., Xu, A., Tang, Y., Shen, L., 2023. Fast Bayesian inference of reparameterized gamma process with random effects. *IEEE Transactions on Reliability* 73, 399–412. doi:[10.1109/TR.2023.3263940](https://doi.org/10.1109/TR.2023.3263940).
- Zhuang, L., Xu, A., Wang, Y., Tang, Y., 2024. Remaining useful life prediction for two-phase degradation model based on reparameterized inverse Gaussian process. *European Journal of Operational Research* 319, 877–890. doi:[10.1016/j.ejor.2024.06.032](https://doi.org/10.1016/j.ejor.2024.06.032).